BRNO UNIVERSITY OF TECHNOLOGY

VYSOKÉ UČENÍ TECHNICKÉ V BRNĚ

FACULTY OF MECHANICAL ENGINEERING

FAKULTA STROJNÍHO INŽENÝRSTVÍ

INSTITUTE OF PHYSICAL ENGINEERING

ÚSTAV FYZIKÁLNÍHO INŽENÝRSTVÍ

ELECTRON BEAM SHAPING VIA INTERACTION WITH OPTICAL NEAR FIELDS

TVAROVÁNÍ ELEKTRONOVÝCH SVAZKŮ POMOCÍ INTERAKCE S BLÍZKÝMI OPTICKÝMI POLI

BACHELOR'S THESIS

BAKALÁŘSKÁ PRÁCE

AUTHOR — Martin Hájek

AUTOR PRÁCE

SUPERVISOR — Ing. Andrea Konečná, Ph.D.

VEDOUCÍ PRÁCE

BRNO 2022

BRNO UNIVERSITY OF TECHNOLOGY
FACULTY OF MECHANICAL ENGINEERING

Assignment Bachelor's Thesis

Institut:	Institute of Physical Engineering
Student:	**Martin Hájek**
Degree programm:	Physical Engineering and Nanotechnology
Branch:	no specialisation
Supervisor:	**Ing. Andrea Konečná, Ph.D.**
Academic year:	2022/23

As provided for by the Act No. 111/98 Coll. on higher education institutions and the BUT Study and Examination Regulations, the director of the Institute hereby assigns the following topic of Bachelor's Thesis:

Electron beam shaping via interaction with optical near fields

Brief Description:

Electron beam shaping is typically performed with the aid of electron–optical elements or specialized diffraction apertures. This work will be focused on one of the alternative methods of electron wave function modulation in the stimulated interaction with photons in the near field. The near field emerging due to the excitation of surface polaritons in selected nanostructures will be modeled within the scope of this work. Finally, modulation of the electron beam after propagation through the optical near field will be calculated.

Bachelor's Thesis goals:

1) Review literature on the topic of the thesis.
2) Model near field corresponding to surface polaritons excited in selected nanostructures.
3) Model the interaction of an electron beam with the near field.

Recommended bibliography:

GARCÍA DE ABAJO, F. J.; DI GIULIO, V. Optical excitations with electron beams: Challenges and opportunities. ACS Photonics. 2021, 8, 945-974.

KONEČNÁ, A.; GARCÍA DE ABAJO, F. J. TSESSES, S.; DAHAN, R.; WANG, K.; REINHARDT, O.; BARTAL, G.; KAMINER, I. Tunable photon-induced spatial modulation of free electrons. arXiv preprint arXiv:2203.08518. 2022.

Deadline for submission Bachelor's Thesis is given by the Schedule of the Academic year2022/23

In Brno,

L. S.

prof. RNDr. Tomáš Šikola, CSc. Director of the Institute	doc. Ing. Jiří Hlinka, Ph.D. FME dean

Abstrakt
Tvarování elektronových svazků je perspektivní metoda, využívající elektron-fotonové interakce. Blízká plazmonová pole mohou zapříčinit modulaci amplitudy a fáze procházející elektronové vlny. Vytvořením analytického modelu interakce elektronu s blízkými plazmonovými poli lze docílit popisu cíleně vytvořených tvarovaných elektronových svazků.

Abstract
Electron beam shaping is a perspective method utilizing electron-photon interaction. Plasmonic optical near-fields modulate the amplitude and phase of traversing electron wave. By creating an analytical model of electron interaction with plasmonic interference patterns, it is possible to inspect the creation of on-demand shaped electron waves.

Klíčová slova
Tvarované elektronové svazky, Elektron-fotonová interakce, Povrchový plazmonový polariton, Interference povrchových plazmonových polaritonů.

Keywords
Shaped electron beams, Electron-photon interaction, Surface plasmon polariton, Surface plasmon polariton interference.

HÁJEK, M. *Electron beam shaping via interaction with optical near fields*. https://www.vut.cz/studenti/zav-prace/detail/150288. Bachelor's thesis. Brno university of technology, Faculty of Mechanical Engineering, Institute of Physical Engineering, 2023. Supervisor Ing. Andrea Konečná, Ph.D.

I declare that this thesis was created by myself, with the scientific supervision of Ing. Andrea Konečná, Ph.D. All references and sources are properly listed in the Bibliography section.

Martin Hájek

Acknowledgements

First and foremost I would like to express my greatest gratitude towards my supervisor Andrea Konečná, for giving me the opportunity to work on such a fascinating topic with a promising perspective. I also very much appreciate the advices, talks, and welcomed critique, because that is what made my thesis much better than it otherwise would be.

I definitely cannot forget to thank my parents for the support they gave me throughout, not only the time writing this thesis but also all the years at university and beyond. Díky Mami, Díky Tati.

Last but not least, thanks to my friends and colleagues in fyzING, especially then.. for the little challenge of ours, to get the word „Medvěd" into our theses

Martin Hájek

Contents

INTRODUCTION

Electron microscopes are one of today's most powerful tools for probing into the complex nanoworld, on which the macroscopic properties of materials substantially depend. Electron microscopy helps us in many seemingly different fields of science. Its sphere of influence ranges from the development in material sciences, all the way to life sciences. Testing and finding new and useful materials that are pushing our technical capabilities forward or watching viruses and bacteria work, in a look for better treatments or ways to appropriate their observed behavior to our advantage.

It is therefore essential to develop and improve the electron imaging technology in order to study various systems, nanostructures, and materials on the atomic scale, but also inspect and control the function of man-made lithographic structures such as transistors and other technologies relying on the processes dependent on physics on atomic level.

One way of improving electron microscopes could be shaping the electron beam itself, i.e., modulating the amplitude of the beam and/or altering the phase of the electron wave. Electron beam-shaping is a new way how to utilize electrons for imaging beyond the limits of conventional methods. Hence it came to wide attention in the last few years and it is getting the interest of many research groups around the world.

The shaped electron beams **(SEBs)** could solve a few essential problems that occur during imaging in the electron microscope, e.g., aberrations. SEBs could even be capable of bringing totally new ways of observing the specimen depending on its unique properties, such as specific resonant energy levels. By utilizing certain symmetries, we may be capable of shaping the beams correspondingly to the material crystallographic structure, which could be useful in inspecting its properties and response.

There are several methods suitable for shaping the electron beams. Each one modulates the amplitude and phase of the electron wave by a slightly different process. State-of-the-art method, which will be described in this thesis is using plasmonic optical near fields [25], specifically the surface plasmon polaritons **(SPPs)**, which are one of the main interests of research in nanophotonics's subfield fittingly called plasmonics. This phenomenon occurs in the case of coupling between free electron gas oscillations in metals, so-called plasmons, to incoming electromagnetic **(EM)** waves - photons, on a metal-dielectric interface.

Our focus is to describe these fields and consider the conditions of their formation, propagation, and interference. If the conditions are met, SPPs may be excited on specific nanostructures on thin metal films. Excited SPPs interfere and, in suitable geometries, generate standing electromagnetic waves. The shape of the SPP interference pattern is determined by the geometry of the interference nanostructure [6]. Note that nanostructures may be relatively easily manufactured into desired geometries giving us a degree of freedom in creating tailored interference patterns.

Ultra-fast electron traversing structured SPP wave patterns interacts with the electric component of the electromagnetic wave and gains or loses quanta of energy [11]. For an electron wave passing through perpendicularly to the film, the main contribution to the energy gains or losses comes from the out-of-plane component of the electric intensity (usually z component of electric intensity, as will be shown later on). In-plane components have a minor effect on the overall shape of out-coming electron wave.

The goal of the thesis is to exploit these facts in creating an analytical model of surface plasmon polariton interference exited by illuminating nanostructures on a thin metal film. Then, the theory of electron-photon interaction will be portrayed and implemented in the model. After computing interfered electromagnetic fields in the interaction region we combine both theories, SPPs, and electron-photon interaction together, which will result in obtaining forms of shaped electron beams - SEBs. The computations of the model take place in MATLAB R2021b software environment as well as function surface plots.

1. Optical near fields

As we mentioned in the introduction, optical near fields can influence the amplitude and phase of the fast electron wave function via electron-photon interaction. This thesis focuses on electrons' interaction with the plasmonic optical near fields. We will therefore describe the quanta of plasma oscillations in metals - plasmons, specifically so-called surface plasmons **(SPs)**, occurring on the metal-dielectric interface. The coupling of SPs with photons gives rise to a quasiparticle called surface plasmon polariton **(SPP)**, which is an electromagnetic wave confined to the metal-dielectric boundary and will play a crucial role in the electron-photon interaction.

We thus first have to describe the physics and theory behind surface waves and electromagnetic waves in general. Maxwell's equations will help us to embark on a rigorous description of SPs and SPPs due to the electromagnetic character of these waves.

1.1. Maxwell's equations

Maxwell's equations in the differential form can be written as:

$$\nabla \cdot \mathbf{D}(\mathbf{r},t) = \rho_{\mathrm{f}}(\mathbf{r},t), \tag{1.1}$$

$$\nabla \cdot \mathbf{B}(\mathbf{r},t) = 0, \tag{1.2}$$

$$\nabla \times \mathbf{E}(\mathbf{r},t) = -\frac{\partial \mathbf{B}(\mathbf{r},t)}{\partial t}, \tag{1.3}$$

$$\nabla \times \mathbf{H}(\mathbf{r},t) = \mathbf{J}_{\mathrm{f}}(\mathbf{r},t) + \frac{\partial \mathbf{D}(\mathbf{r},t)}{\partial t}, \tag{1.4}$$

where $\mathbf{E}, \mathbf{D}$ are electric components of the field, $\mathbf{H}, \mathbf{B}$ being magnetic components, intensity, and induction, respectively. ρ_{f} is free charge density and $\mathbf{J}_{\mathrm{f}}$ free current density. Maxwell's equations have a simpler form in a vacuum. In describing electromagnetic fields in a material environment, however, the following additional relations apply:

$$\mathbf{D}(\mathbf{r},t) = \varepsilon_0 \mathbf{E}(\mathbf{r},t) + \mathbf{P}(\mathbf{r},t), \tag{1.5}$$

and

$$\mathbf{H}(\mathbf{r},t) = \frac{1}{\mu_0}\mathbf{B}(\mathbf{r},t) - \mathbf{M}(\mathbf{r},t), \tag{1.6}$$

where $\mathbf{P}$, $\mathbf{M}$ are polarization and magnetization, respectively. ε_0 is vacuum permittivity and μ_0 vacuum permeability. Polarization describes how difficult it is to polarise the material by an external electric field, while magnetization describes the response to an external magnetic field.

If ε, μ is defined as dielectric function and relative permeability, respectively, we can write $\mathbf{D}$ and $\mathbf{H}$ in this form:

$$\mathbf{D} = \varepsilon_0 \varepsilon \mathbf{E}, \tag{1.7}$$

$$\mathbf{B} = \mu_0 \mu \mathbf{H}. \tag{1.8}$$

The relation between electric field and current density can be expressed via Ohm's law in vector form: $\mathbf{J} = \sigma \mathbf{E}$, where σ is material-dependent conductivity. With those relations, we are completing Maxwell's equations.

1.1.1. Wave equations

Following equations express the wavelike behavior of electric and magnetic fields. By applying curl on equations (1.3) and (1.4) and using the constitutive relations (1.5) and (1.6), we retrieve:

$$\nabla \times \nabla \times \mathbf{E} + \frac{1}{c^2}\frac{\partial^2 \mathbf{E}}{\partial t^2} = -\mu_0 \frac{\partial}{\partial t}\left(\frac{\partial \mathbf{P}}{\partial t} + \mathbf{J}_\mathrm{f} + \nabla \times \mathbf{M}\right). \tag{1.9a}$$

Similarly for magnetic field:

$$\nabla \times \nabla \times \mathbf{H} + \frac{1}{c^2}\frac{\partial^2 \mathbf{H}}{\partial t^2} = \nabla \times \mathbf{J}_\mathrm{f} + \nabla \times \left(\frac{\partial \mathbf{P}}{\partial t}\right) - \frac{1}{c^2}\frac{\partial^2 \mathbf{M}}{\partial t^2}, \tag{1.9b}$$

where $c = 1/\sqrt{\varepsilon_0 \mu_0}$ is the speed of light in vacuum. Equations. (1.9a) and (1.9b) can be simplified using vector calculus identity

$$\nabla \times \nabla \times \mathbf{A} = \nabla(\nabla \cdot \mathbf{A}) - \nabla^2 \mathbf{A}.$$

We consider variation of polarization and magnetization with time to be negligible, as well as $\rho_\mathrm{f} = 0$, $\mathbf{J}_\mathrm{f} = \mathbf{0}$. Furthermore, if we include dielectric function ε and relative permeability μ, provided that it varies insignificantly in space relative to the used light wavelength, we get:

$$\nabla^2 \mathbf{E} - \frac{\varepsilon\mu}{c^2}\frac{\partial^2 \mathbf{E}}{\partial t^2} = 0, \tag{1.10a}$$

and

$$\nabla^2 \mathbf{H} - \frac{\varepsilon\mu}{c^2}\frac{\partial^2 \mathbf{H}}{\partial t^2} = 0. \tag{1.10b}$$

1.1.2. Boundary conditions

Since we will be discussing electromagnetic waves on surfaces, it is desirable to describe fields on the boundary between two different media. Discontinuity of materials implies the existence of certain boundary conditions, which the electromagnetic fields follow. By using divergence (Gauss-Ostrogradsky) theorem and Stokes' theorem one gets Maxwell's equations in integral form, which are more suitable for this problem:

$$\oiint_S \mathbf{D} \cdot \mathrm{d}\mathbf{S} = Q_\mathrm{f}, \tag{1.11}$$

$$\oiint_S \mathbf{B} \cdot \mathrm{d}\mathbf{S} = 0, \tag{1.12}$$

$$\oint_{\partial S} \mathbf{E} \cdot \mathrm{d}\boldsymbol{l} = -\frac{\mathrm{d}}{\mathrm{d}t} \iint_S \mathbf{B} \cdot \mathrm{d}\mathbf{S}, \tag{1.13}$$

$$\oint_{\partial S} \mathbf{H} \cdot \mathrm{d}\boldsymbol{l} = I_\mathrm{f} + \frac{\mathrm{d}}{\mathrm{d}t} \iint_S \mathbf{D} \cdot \mathrm{d}\mathbf{S}, \tag{1.14}$$

where Q_f is free charge closed by any Gauss's surface S and I_f are free currents passing through any surface S bounded by a closed loop ∂S.

By constructing a cylinder of equal bases reaching from one medium to another with its height approaching zero and applying it to (1.11), we get the following relation [12]:

$$\mathbf{n} \cdot (\mathbf{D}_1 - \mathbf{D}_2) = \sigma_\mathrm{f}, \tag{1.15}$$

where $\mathbf{D}_1, \mathbf{D}_2$ are electric induction in region 1 and 2. $\mathbf{n}$ is defined as unit normal vector of surface S pointing from medium 1 to medium 2. σ_f is free surface charge density. Eq. (1.15) tells us that perpendicular components of $\mathbf{D}$ follow:

$$D_1^\perp - D_2^\perp = \sigma_\mathrm{f}. \tag{1.16}$$

Analogously with (1.12) we get:

$$\mathbf{n} \cdot (\mathbf{B}_1 - \mathbf{B}_2) = 0, \qquad B_1^\perp - B_2^\perp = 0. \tag{1.17}$$

In the case of (1.13) and (1.14), we construct a closed loop of rectangular shape, with its two sides parallel to the interface, reaching from one material to another with neglecting height.

$$\mathbf{n} \times (\mathbf{E}_1 - \mathbf{E}_2) = \mathbf{0}, \qquad \mathbf{E}_1^\parallel - \mathbf{E}_2^\parallel = \mathbf{0}, \tag{1.18}$$

$$\mathbf{n} \times (\mathbf{H}_1 - \mathbf{H}_2) = \mathbf{K}_\mathrm{f}, \qquad \mathbf{H}_1^\parallel - \mathbf{H}_2^\parallel = \mathbf{K}_\mathrm{f}, \tag{1.19}$$

where $\mathbf{K}_\mathrm{f}$ is free surface current density. $\mathbf{E}_i^\parallel$, $\mathbf{H}_i^\parallel$ are components parallel to the interface.

1.2. Electromagnetic response of metals

Metals are a specific type of material with so-called metallic bonding of atoms. According to the free electron model (or Drude model), positively charged nuclei of atoms generate the rigid lattice, whereas valence electrons are delocalized and move freely through the bulk of the metal [16]. We call all the electrons in the bulk the conduction electron gas or electron sea.

The optical response of metals is described by complex relative permittivity, also called dielectric function ε. Moreover, in the case of magnetic material we capture its magnetic response in the relative permeability μ.

Now let's take a closer look at the electron behavior in metal. Generally, the motion of electrons in the bulk of the metal is very chaotic, meaning that all sorts of interactions occur, such as Coulomb interaction between electrons, scattering on the atoms in the lattice, etc. This motion of an individual electron would be very difficult to describe. We thus need to simplify the problem.

It turns out that one can depict this system of electrons with a classical statistical view. We assume that the electrons, of effective mass m, move freely until they scatter on average once per time τ, which also characterizes collision frequency $\gamma = \frac{1}{\tau}$, which can be related to an effective damping rate. This whole system creates an electron sea, which is responsive to an external electric field $\mathbf{E}(t)$ and for which we can write an equation of motion:

$$m\frac{\partial^2 \mathbf{r}(t)}{\partial t^2} + m\gamma\frac{\partial \mathbf{r}(t)}{\partial t} = -e\mathbf{E}(t), \tag{1.20}$$

where $\mathbf{r}(t)$ is a displacement of electron. Provided that the driving electric field $\mathbf{E}$ is harmonic, that is $\mathbf{E}(t) \propto \mathrm{e}^{-\mathrm{i}\omega t}$, where ω is angular frequency, solution for (1.20) is

$$\mathbf{r}(t) = \frac{e}{m(\omega^2 + \mathrm{i}\gamma\omega)}\mathbf{E}(t). \tag{1.21}$$

Electron displacement contributes to polarization as $\mathbf{P} = -ne\mathbf{r}$, where n is the charge carrier density so we get:

$$\mathbf{P}(t) = -\frac{ne^2}{m(\omega^2 + \mathrm{i}\gamma\omega)}\mathbf{E}(t), \tag{1.22}$$

which via Eq. (1.5) leads to:

$$\mathbf{D}(t) = \varepsilon_0\left(1 - \frac{\omega_\mathrm{p}^2}{\omega^2 + \mathrm{i}\gamma\omega}\right)\mathbf{E}(t), \tag{1.23}$$

where $\omega_\mathrm{p} = \sqrt{ne^2/(m\varepsilon_0)}$ is called the plasma frequency. Comparing Eq. (1.23) to Eq. (1.7) provides an expression for a frequency-dependent dielectric function

$$\varepsilon(\omega) = 1 - \frac{\omega_\mathrm{p}^2}{\omega^2 + \mathrm{i}\gamma\omega}. \tag{1.24}$$

1.3. Plasmons and surface plasmon polaritons

By definition, plasmons are quasiparticles representing quanta of collective charge density oscillations [20]. Special role have surface plasmons, which appear on the interface between metal and dielectric.

SPPs are electromagnetic waves traveling along a metal-dielectric interface, evanescently decaying in the perpendicular direction to the interface, with propagation lengths up to tens of micrometers [2]. Because they arise from the coupling of light to charge oscillations, they have few unique properties, which will be apparent from their dispersion relation (Fig. 1.2).

1.3.1. Surface waves - Electromagnetic field components

From now on, we assume non-magnetic media, i.e. $\mu = 1$, therefore $\mathbf{B} = \mu_0 \mathbf{H}$. Relations for surface waves can be derived from EM field component relations, which can be expressed from Eqs. (1.3) and (1.4):

$$\frac{\partial H_z}{\partial y} - \frac{\partial H_y}{\partial z} = -\mathrm{i}\omega\varepsilon_0\varepsilon E_x, \qquad \frac{\partial E_z}{\partial y} - \frac{\partial E_y}{\partial z} = -\mathrm{i}\omega\mu_0 B_x, \tag{1.25}$$

$$\frac{\partial H_x}{\partial z} - \frac{\partial H_z}{\partial x} = -\mathrm{i}\omega\varepsilon_0\varepsilon E_y, \qquad \frac{\partial E_x}{\partial z} - \frac{\partial E_z}{\partial x} = -\mathrm{i}\omega\mu_0 B_y, \tag{1.26}$$

$$\frac{\partial H_y}{\partial x} - \frac{\partial H_x}{\partial y} = -\mathrm{i}\omega\varepsilon_0\varepsilon E_z, \qquad \frac{\partial E_y}{\partial x} - \frac{\partial E_x}{\partial y} = -\mathrm{i}\omega\mu_0 B_z. \tag{1.27}$$

Additionally, we will describe the surface waves with the help of wave equations (1.10a), (1.10b). The assumption of harmonic dependence of the fields $\mathbf{E}(\mathbf{r}, t) = \mathbf{E}(\mathbf{r})\mathrm{e}^{-\mathrm{i}\omega t}$ yields the Helmholtz equations:

$$\nabla^2\mathbf{E} + k_0^2\varepsilon\mathbf{E} = 0, \tag{1.28a}$$

$$\nabla^2\mathbf{H} + k_0^2\varepsilon\mathbf{H} = 0, \tag{1.28b}$$

where $k_0 = \omega/c$ is free-space photon dispersion relation.

1.4. SPPs on the interface of two media

To describe the SPPs on the interface, we first need to define the geometry. We divide the space into two separate regions at $z = 0$ with dielectric in $z > 0$ and metal in $z < 0$. We consider wave propagating parallel with the x axis.

There are two possible polarizations of the wave. The TE polarization is transversal electric with electric components $(0, E_y, 0)$ and magnetic components $(H_x, 0, H_z)$. The second polariza-

tion is TM - transversal magnetic, where nonzero components are H_y for the magnetic field and E_x, E_z for electric. It can be shown that SPPs cannot exist in TE polarization (Appendix 3.3.2), we will thus calculate with TM polarization only. Due to the geometry of propagation and TM polarization (1.25) can be simplified as

$$E_x = -\mathrm{i}\frac{1}{\omega\varepsilon_0\varepsilon}\frac{\partial H_y}{\partial z}, \tag{1.29a}$$

$$E_z = \mathrm{i}\frac{1}{\omega\varepsilon_0\varepsilon}\frac{\partial H_y}{\partial x}. \tag{1.29b}$$

SPPs are confined to the interface, evanescently decaying in the z direction. The solution for such a wave therefore is:

$$H_y = A\mathrm{e}^{\mathrm{i}(k_x x-\omega t)}\mathrm{e}^{\pm\alpha z}, \tag{1.30}$$

where k_x is the x component of wavevector, A amplitude and α is the decay coefficient.
$\pm$ denotes solution for $z>0$, which leads to $\mathrm{e}^{-\alpha z}$ and for $z<0$, for which we use $\mathrm{e}^{+\alpha z}$.

Using Eq. (1.30) and adding E_x, E_z components from (1.29), we obtain expressions describing fields in both regions I and II denoted by index $i=1,2$, respectively. We assign ε_i and α_i to each region, A_1, A_2 are amplitudes. In the $z>0$ half-space, we have $i=2$, and electromagnetic field described as:

$$H_y^{II}(z,t) = A_2\mathrm{e}^{\mathrm{i}(k_x x-\omega t)}\mathrm{e}^{-\alpha_2 z}, \tag{1.31}$$

$$E_x^{II}(z,t) = \mathrm{i}A_2\frac{1}{\omega\varepsilon_0\varepsilon_2}\alpha_2\mathrm{e}^{\mathrm{i}(k_x x-\omega t)}\mathrm{e}^{-\alpha_2 z}, \tag{1.32}$$

$$E_z^{II}(z,t) = -A_2\frac{k_x}{\omega\varepsilon_0\varepsilon_2}\mathrm{e}^{\mathrm{i}(k_x x-\omega t)}\mathrm{e}^{-\alpha_2 z}. \tag{1.33}$$

For the other half-space, where $z<0$ and $i=1$, we find

$$H_y^{I}(z,t) = A_1\mathrm{e}^{\mathrm{i}(k_x x-\omega t)}\mathrm{e}^{\alpha_1 z}, \tag{1.34}$$

$$E_x^{I}(z,t) = -\mathrm{i}A_1\frac{1}{\omega\varepsilon_0\varepsilon_1}\alpha_1\mathrm{e}^{\mathrm{i}(k_x x-\omega t)}\mathrm{e}^{\alpha_1 z}, \tag{1.35}$$

$$E_z^{I}(z,t) = -A_1\frac{k_x}{\omega\varepsilon_0\varepsilon_1}\mathrm{e}^{\mathrm{i}(k_x x-\omega t)}\mathrm{e}^{\alpha_1 z}. \tag{1.36}$$

In Fig. 1.1 we can see magnetic component of SPP in vacuum $z > 0$ on metal $z < 0$.

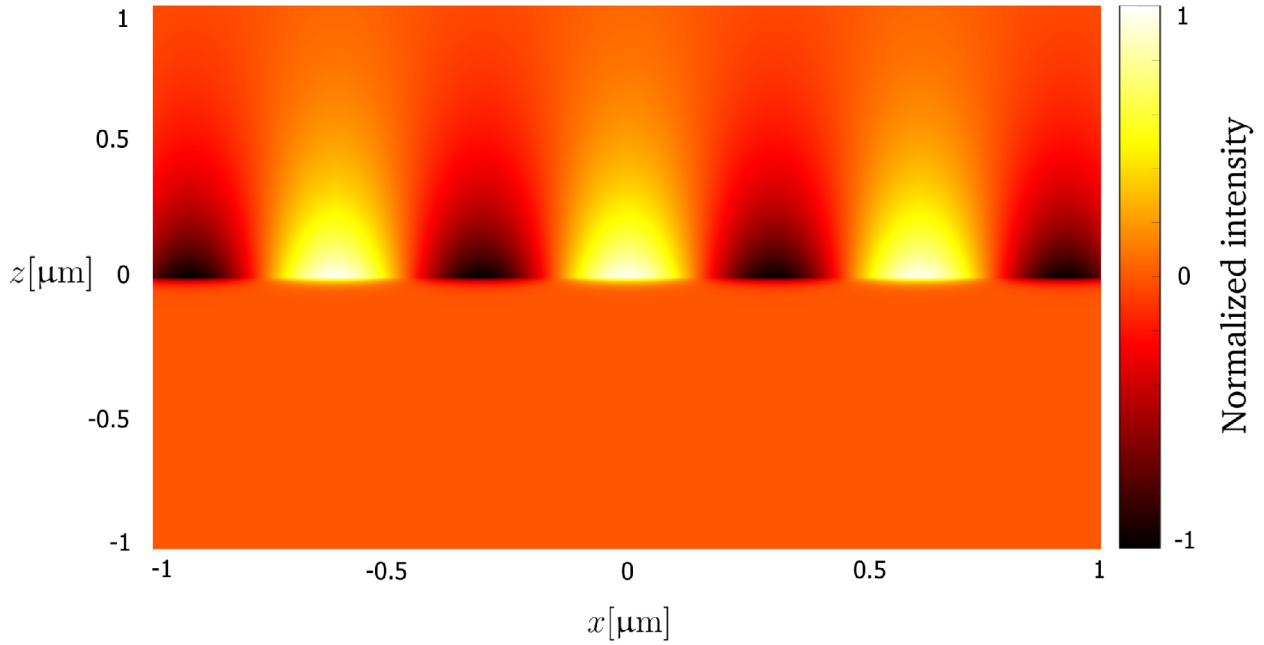

Figure 1.1: SPP normalized component of intensity H_y on single vacuum-metal interface. Frequency $\omega = 3 \cdot 10^{15}\,\mathrm{rad} \cdot \mathrm{s}^{-1}$, plasma frequency for gold $\omega_p = 1.37 \cdot 10^{16}\,\mathrm{rad} \cdot \mathrm{s}^{-1}$ and $\gamma = 7.14 \cdot 10^{13}\,\mathrm{rad} \cdot \mathrm{s}^{-1}$.

Solutions for SPPs in TM polarization do exist. However, certain conditions must be fulfilled. At $z = 0$ according to Eq. (1.19) $\mathbf{H}^{\parallel}$ must be continuous in the case of zero surface current density, that implies condition for amplitudes, i.e., $A_1 = A_2$. Moreover the electric components $\mathbf{E}^{\parallel}$, due to Eq. (1.18), give us the condition:

$$-\frac{\alpha_2}{\varepsilon_2} = \frac{\alpha_1}{\varepsilon_1}. \tag{1.37}$$

Because $\mathrm{Re}\{\alpha_i > 0\}$ for both media, the only possible solution is that $\varepsilon_2 > 0$ is a dielectric and the second medium has $\mathrm{Re}\{\varepsilon_1\} < 0$, which is satisfied by metals. And last but not least, the dispersion relation for wave vector can be obtained using Eq. (1.28b):

$$\alpha_2^2 = k_x^2 - k_0^2 \varepsilon_2, \tag{1.38a}$$

$$\alpha_1^2 = k_x^2 - k_0^2 \varepsilon_1. \tag{1.38b}$$

If we substitute the relations (1.38) into Eq. (1.37) we get the dispersion relation (Fig. 1.2):

$$k_x = k_0 \sqrt{\frac{\varepsilon_1 \varepsilon_2}{\varepsilon_1 + \varepsilon_2}}. \tag{1.39}$$

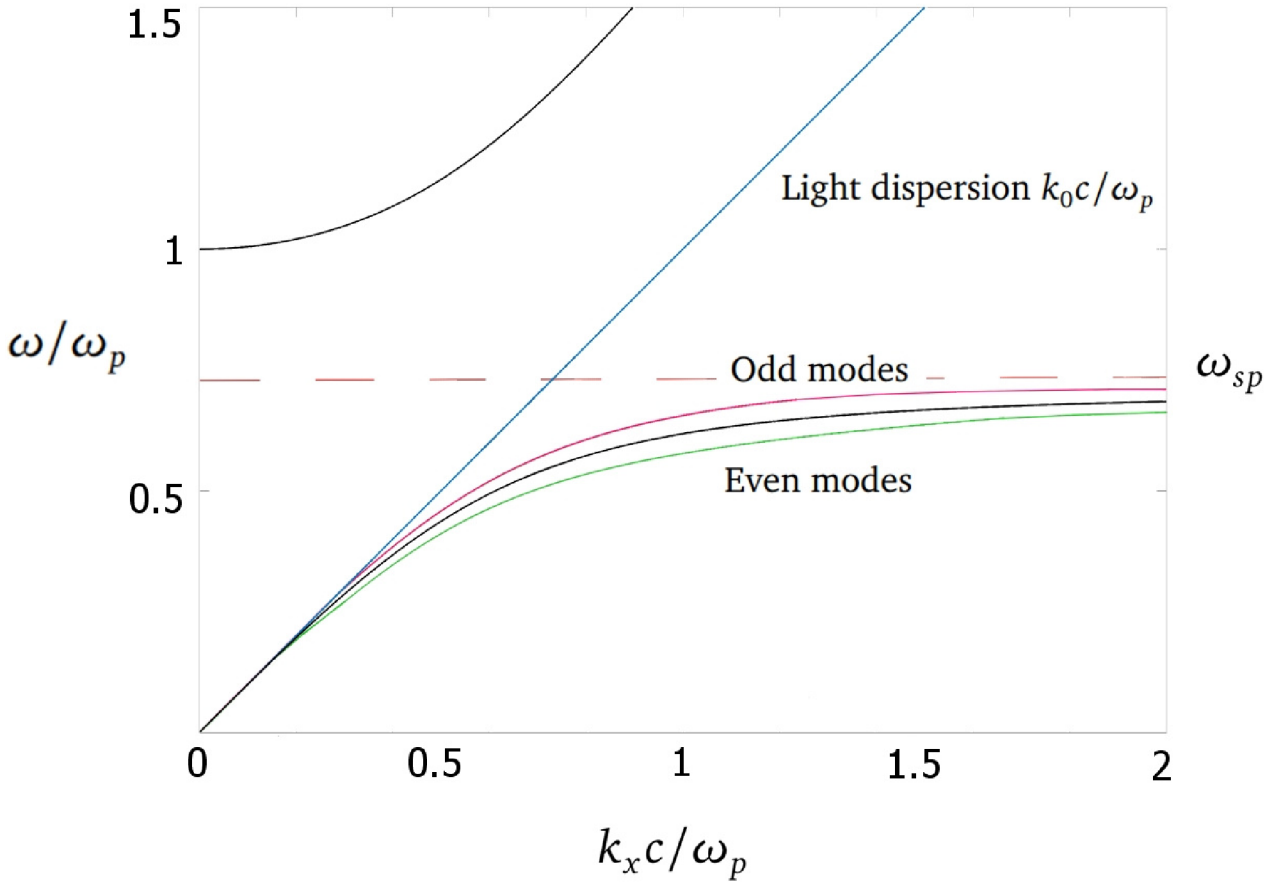

Figure 1.2: Dispersion relation of SPP from Eq. (1.39) is represented by black curve below ω_p. Black curve above ω_p represents so-called Brewster mode. The blue line describes the dispersion relation of light. Odd and even modes describe the dispersion in the case of Eqs. (1.52), (1.51). Here we do not consider any damping i.e. $\mathrm{Im}\{\varepsilon_1\} = 0$.

In the limit of large k_x, Eq. (1.39) can be rewritten with the use of Eq. (1.24) and assuming negligible damping ($\gamma \to 0$). The characteristic frequency of surface plasmon therefore can be expressed as

$$\omega_{\mathrm{sp}} = \frac{\omega_p}{\sqrt{1+\varepsilon_2}}. \tag{1.40}$$

1.5. SPPs in a thin film

Now we move on to a more complex geometry. We take an infinite metal film, with confinement in the z axis. We assume the thickness $2a$ in z direction, which should be in order of few tens of nanometers, because later on we will be considering electrons passing through the film, which requires films around tens of nanometers in thickness. Otherwise, the electrons would significantly deviate from their original path [15]. The center of the coordinate system is in the middle of the film, which is surrounded by a vacuum or dielectric on both sides.

Furthermore, for simplicity of the model, we assume that the medium in the region III and medium in the region II (see Fig. 1.3) are the same, i.e. $\varepsilon_3 = \varepsilon_2$, which also implies $\alpha_3 = \alpha_2$. Description of time dependence was counted for with the term capturing harmonic time variation $e^{-i\omega t}$, but for better readability from now on, we look at the time $t = 0$, while keeping in mind that time dependence can always be added to the equations.

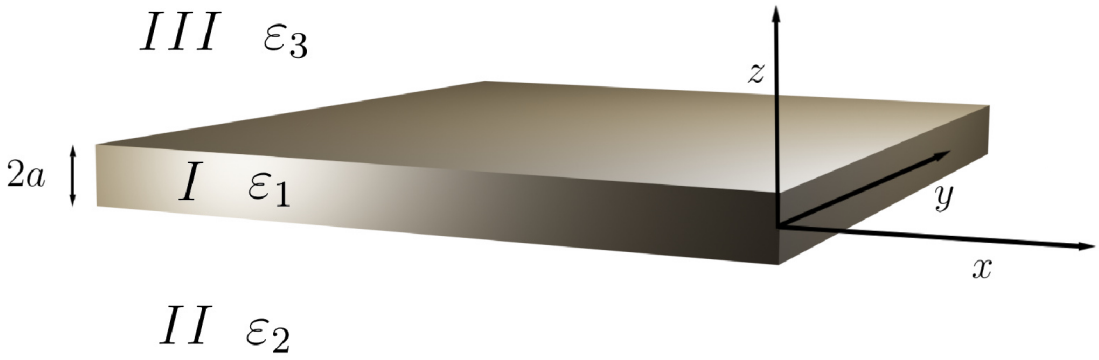

Figure 1.3: Air/metal/air model, the thickness of the film is $2a$. The origin of z is in the middle of the film.

The electromagnetic components of SPPs will be very similar in form to the previous case with one interface. Note that two SPPs arise at each adjacent boundary in the case of two interfaces. Moreover, these SPPs are coupled, and one depends on the other.

For region I, that is $-a < z < a$, there are going to be contributions from SPPs from each boundary of the film due to coupling [20]. The first one decaying in z and the second in $-z$:

$$H_y^I = Ce^{ik_x x}e^{\alpha_1 z} + De^{ik_x x}e^{-\alpha_1 z}, \tag{1.41}$$

$$E_x^I = -iC\frac{1}{\omega\varepsilon_0\varepsilon_3}\alpha_1 e^{ik_x x}e^{\alpha_1 z} + iD\frac{1}{\omega\varepsilon_0\varepsilon_1}\alpha_1 e^{ik_x x}e^{-\alpha_1 z}, \tag{1.42}$$

$$E_z^I = C\frac{k_x}{\omega\varepsilon_0\varepsilon_1}e^{ik_x x}e^{\alpha_1 z} + D\frac{k_x}{\omega\varepsilon_0\varepsilon_1}e^{ik_x x}e^{-\alpha_1 z}. \tag{1.43}$$

In the half-space above the metallic film/slab ($z > a$, region III), the electromagnetic field is expressed as:

$$H_y^{III} = A\mathrm{e}^{\mathrm{i}k_x x}\mathrm{e}^{-\alpha_3 z}, \tag{1.44}$$

$$E_x^{III} = \mathrm{i}A\frac{1}{\omega\varepsilon_0\varepsilon_3}\alpha_3\mathrm{e}^{\mathrm{i}k_x x}\mathrm{e}^{-\alpha_3 z}, \tag{1.45}$$

$$E_z^{III} = -A\frac{k_x}{\omega\varepsilon_0\varepsilon_3}\mathrm{e}^{\mathrm{i}k_x x}\mathrm{e}^{-\alpha_3 z}, \tag{1.46}$$

while below the film/slab ($z < -a$, region II), we obtain

$$H_y^{II} = B\mathrm{e}^{\mathrm{i}k_x x}\mathrm{e}^{\alpha_2 z}, \tag{1.47}$$

$$E_x^{II} = \mathrm{i}B\frac{1}{\omega\varepsilon_0\varepsilon_2}\alpha_2\mathrm{e}^{\mathrm{i}k_x x}\mathrm{e}^{\alpha_2 z}, \tag{1.48}$$

$$E_z^{II} = -B\frac{k_x}{\omega\varepsilon_0\varepsilon_2}\mathrm{e}^{\mathrm{i}k_x x}\mathrm{e}^{\alpha_2 z}. \tag{1.49}$$

Using the continuity of H_y and E_x on boundaries, we get a system of linear equations for complex amplitudes A, B, C, D:

$$\begin{pmatrix} \mathrm{e}^{-\alpha_3 a} & 0 & -\mathrm{e}^{\alpha_1 a} & -\mathrm{e}^{-\alpha_1 a} \\ (\alpha_3/\varepsilon_3)\mathrm{e}^{-\alpha_3 a} & 0 & (\alpha_1/\varepsilon_1)\mathrm{e}^{\alpha_1 a} & -(\alpha_1/\varepsilon_1)\mathrm{e}^{-\alpha_1 a} \\ 0 & \mathrm{e}^{-\alpha_2 a} & -\mathrm{e}^{-\alpha_1 a} & -\mathrm{e}^{\alpha_1 a} \\ 0 & -(\alpha_2/\varepsilon_2)\mathrm{e}^{-\alpha_2 a} & (\alpha_1/\varepsilon_1)\mathrm{e}^{-\alpha_1 a} & -(\alpha_1/\varepsilon_1)\mathrm{e}^{\alpha_1 a} \end{pmatrix} \begin{pmatrix} A \\ B \\ C \\ D \end{pmatrix} = \begin{pmatrix} 0 \\ 0 \\ 0 \\ 0 \end{pmatrix}. \tag{1.50}$$

Furthermore in the computational model we will set A as an unit of amplitude and express other amplitudes B, C, D in terms of A. This helps us better fit the model to experimental data of illumination strength, which directly determines the intensities.

1.5.1. Coupled SPP modes

Boundary conditions with wave equations also give necessary conditions for coupled surface plasmon polaritons on both interfaces. We get two eigenmodes from solving $\det(M) = 0$, where M is 4×4 matrix from Eq. (1.50):

$$\tanh(\alpha_1 a) = -\frac{\alpha_2 \varepsilon_1}{\alpha_1 \varepsilon_2}, \tag{1.51}$$

$$\tanh(\alpha_1 a) = -\frac{\alpha_1 \varepsilon_2}{\alpha_2 \varepsilon_1}, \tag{1.52}$$

which represent two modes for SPPs, odd and even functions, respectively (See Fig. 1.4). In odd parity E_x is odd function and H_y, E_z are even functions (odd/even notation in correspondence with [20]).
Using

$$\alpha_i = \sqrt{k_x^2 - k_0^2 \varepsilon_i}, \tag{1.53}$$

Eqs. (1.51) and (1.52) can be rewritten as functions of k_x. The equations are then solved for k_x, numerically, yielding dispersions of SPP modes. (for purposes of this Thesis, it was solved with the help of MATLAB R2021b `fsolve()` function, Fig. 1.2):

$$\tanh\left(a\sqrt{k_x^2 - k_0^2 \varepsilon_1}\right) + \frac{\varepsilon_1 \sqrt{k_x^2 - k_0^2 \varepsilon_2}}{\varepsilon_2 \sqrt{k_x^2 - k_0^2 \varepsilon_1}} = 0, \tag{1.54}$$

and

$$\tanh\left(a\sqrt{k_x^2 - k_0^2 \varepsilon_1}\right) + \frac{\varepsilon_2 \sqrt{k_x^2 - k_0^2 \varepsilon_1}}{\varepsilon_1 \sqrt{k_x^2 - k_0^2 \varepsilon_2}} = 0. \tag{1.55}$$

In the limit $a \to \infty$, from Eqs. (1.51), (1.52) we get the expression we obtained earlier for an SPP at a single interface (1.37).

We may also define the propagation length of SPP, which is determined by the imaginary part of k_x and represents the length from the origin of SPP to the point where the intensity decays to 1/e multiple of its original intensity [2]:

$$L = \frac{1}{2\mathrm{Im}\{k_x\}}. \tag{1.56}$$

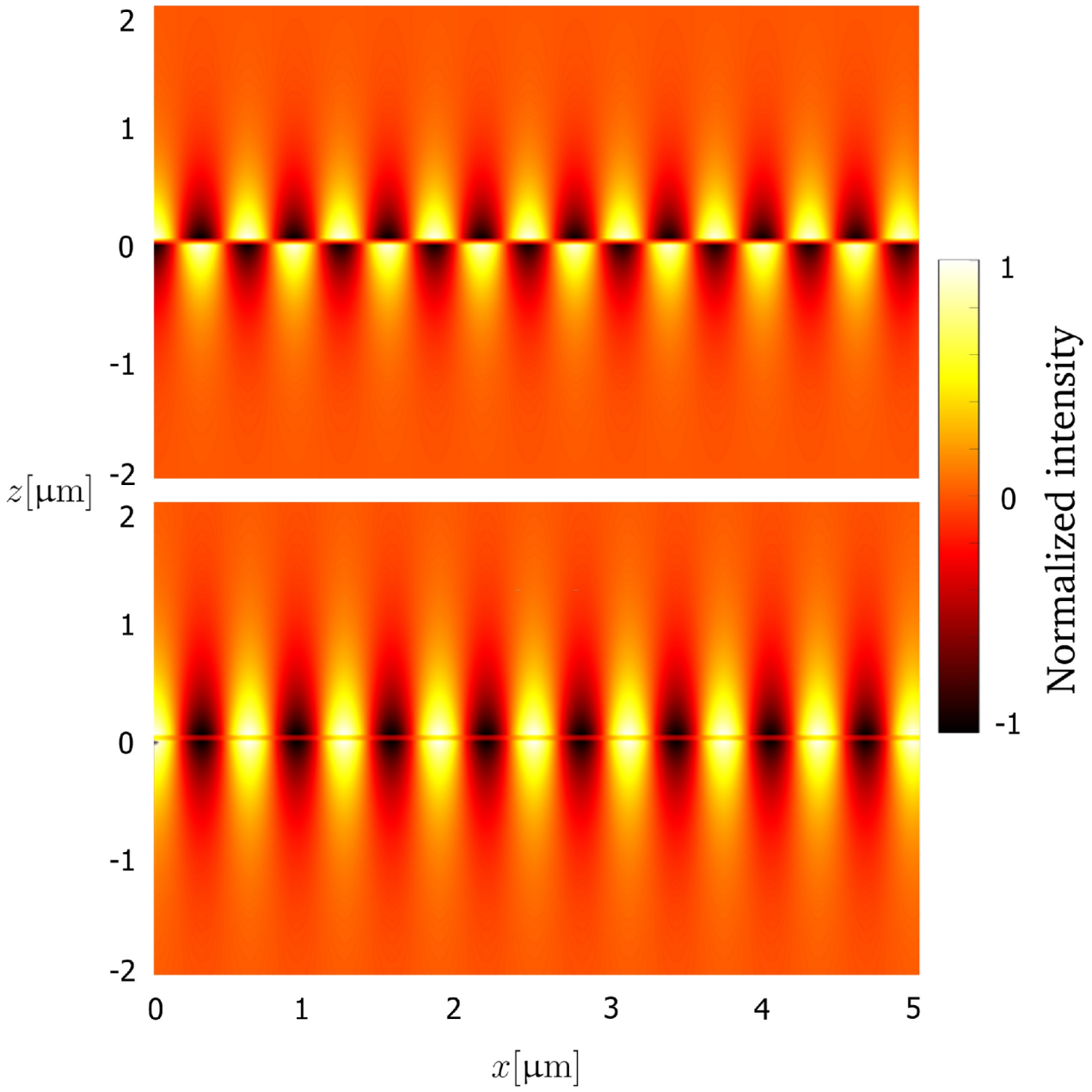

Figure 1.4: Surface plasmon polaritons at vacuum-metal-vacuum setup. Color scale shows normalized intensity H_y of even and odd mode, for the film thickness of 60 nm, frequency $\omega = 3 \cdot 10^{15}\,\mathrm{rad} \cdot \mathrm{s}^{-1}$, plasma frequency of gold $\omega_p = 1.37 \cdot 10^{16}\,\mathrm{rad} \cdot \mathrm{s}^{-1}$, and "damping expressed by $\gamma = 7.14 \cdot 10^{13}\,\mathrm{rad} \cdot \mathrm{s}^{-1}$.

1.5.2. SPP excitations

Due to the mismatch in the wavevector of SPPs and light (see Fig. 1.2), SPPs cannot be excited by light on the plain metal-air interface. SPPs are also bound to the surface and do not propagate perpendicularly to the interface. Non-triviality of the excitation requires special configurations such as methods involving total internal reflection [27]. Excitation of SPPs may also be achieved by illuminating certain nanostructures, which means, that incident light on these nanostructures is converted into SPPs [23]. Methods, which use nanostructure illumination, are more appropriate for our use since the sources of SPPs happen to be nanostructures such as grating, grooves, and slits in thin metal films, which are easier to implement into the analytical model.

Particularly the efficiency of groove SPP excitations can furthermore be tuned by the geometry of the groove itself [23]. We can thus consider these nanostructures as valid and tunable sources of SPPs, if illuminated, and use them in the analytical model by defining their position, therefore defining the coordinates of the SPP source.

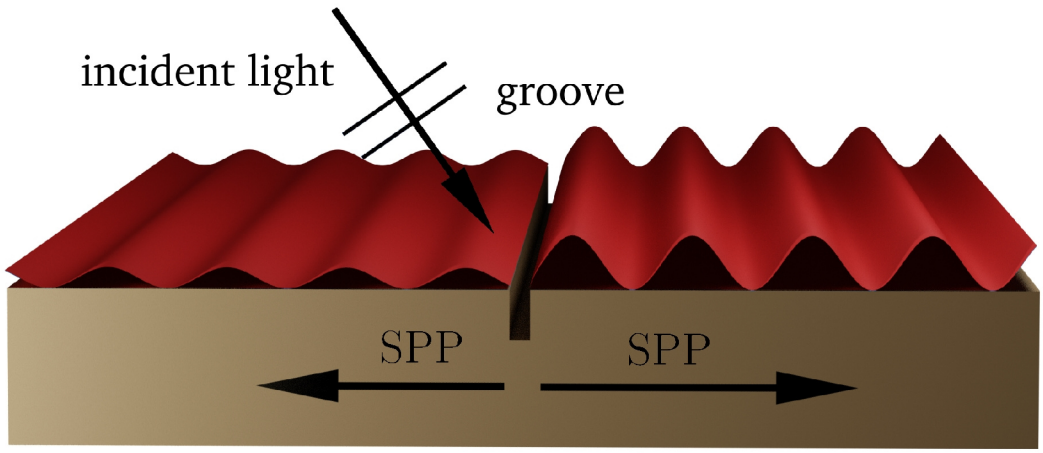

Figure 1.5: Scheme of SPP excitation on the groove. Incident plane electromagnetic wave excites SPP at the groove, which then propagates outwards, while bound to the surface. Note, that SPPs propagate in both directions off of the groove, though we will be interested in the one, that propagates towards the interference region .

2. Interference model of surface plasmon polaritons

2.1. Surface wave sources

The basic groundwork of plasmonic near fields has been set for us to move on to the description of the interference of SPPs. In the model, the source of SPPs is defined via its coordinates and the amplitude of an outgoing surface wave.

The length of grooves or slits, which can be sources of SPPs, is a characteristic dimension and long relative to their other dimensions. It is, therefore, suitable for the model to consider arising SPPs as plane waves, under the limit of long enough sources of SPPs and consideration, that the outgoing plane wave covers the whole desired interference region. This way, the diffraction on the edges of the source is not going to affect the interference in this region.

For SPPs in the metal film, we will use the odd mode, represented by Eq. (1.52), because of the longer propagation length of this mode (1.56) [2]. But it is possible to change the characteristics in the computation according to our specific needs or potential future experimental setup.

2.2. Interference of E_z fields

Interference of multiple SPPs can be described as a total sum of all contributions from each source. SPP field components are described by a set of relations: (1.41)-(1.49). We will mainly focus on E_z components since those are essential in describing electron-photon interaction, which will be discussed later. It is also important to note that interference of the SPPs propagating in opposite directions gives rise to standing waves [6]. Since the interference will occur on the XY plane, wavevector k_x will further be split into new x component $k_x^{'}$ and y component $k_y^{'}$ based on the direction of propagation of each source on the XY plane, i.e. the expression $e^{ik_x x}$ transforms into $e^{i(k_x^{'}x+k_y^{'}y)}$, we additionally define $K = \sqrt{k_x^{'2}+k_y^{'2}}$. The z component of electric intensity can be described in all three regions III, I, II, respectively:

$$E_z^{III}(x,y,z) = -A\frac{K}{\omega\varepsilon_0\varepsilon_3}e^{i(k_x^{'}x+k_y^{'}y)}e^{-\alpha_3 z}, \tag{2.1}$$

$$E_z^{I}(x,y,z) = \left(Ce^{\alpha_1 z}+De^{-\alpha_1 z}\right)\frac{K}{\omega\varepsilon_0\varepsilon_1}e^{i(k_x^{'}x+k_y^{'}y)}, \tag{2.2}$$

$$E_z^{II}(x,y,z) = -B\frac{K}{\omega\varepsilon_0\varepsilon_2}e^{i(k_x^{'}x+k_y^{'}y)}e^{\alpha_2 z}. \tag{2.3}$$

As was stated, the total value of E_z in one point in space is the sum of contributions from each source, the sum is separate for each region ($R = III, I$ or I), we also define $x_j = x - x_0$, $y_j = y - y_0$, where x_0, y_0 are coordinates of the SPP source center. Corresponding wavectors will be denoted $k_{x,j}$ and $k_{y,j}$

$$E^R_{z,\mathrm{tot}}(x,y,z) = \sum_{\text{source } j} E^R_{z,j}(x_j, y_j, z) \tag{2.4}$$

The intensities of the SPP risen at the coordinates of the groove can also be adjusted. The adjustment happens via the settings of amplitudes from Eq. (1.50), in order to correspond to experimental data of illumination strength.

2.3. Interference geometries

Created SPP interference patterns are dependent on the specific geometry of the interference structure which we refer to as surface plasmon interference device **(SPID)** [4] [5] and we may thus design the SPP patterns accordingly to this fact. It is desirable to respect specific symmetrical arrangements of SPIDs such as hexagonal, square, etc. It will come useful later in modulating desired forms of SEBs.

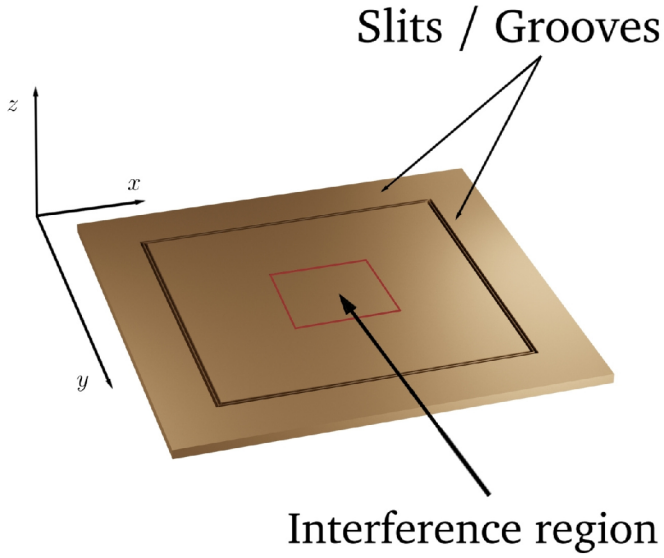

Figure 2.1: Possible interference structure representing square arrangement.

In the model, the coordinate system origin is in the middle of the thin film, which is parallel to the XY plane, analogous to 1.3.

Fig. 2.2 shows the function of the model in detail, grooves are sources, which are defined by a) distance (radius) r away from the center, b) angle θ between the line, from origin to groove center, and x axis. And c) by their length l, which in projection towards the center covers the

interference region. The interference region is in the center. Note that this figure shows only one of the possible arrangements and all of the factors (number of grooves, length l, distance r, angle θ) are adjustable to a form for creating the desired interference patterns.

2.4. Resulting patterns

Figures 2.3 - 2.6 show SPP interference from different geometries of SPID, which result in two-dimensional periodic patterns, which have characteristic features in correspondence to the SPID geometry. That might be useful in creating tailored SEBs with these specific patterns, for example, hexagonal for the study of materials, whose structure shows such symmetry.

SPPs are here represented by E_z component right at the film surface in the region III (Fig. 1.3), i.e. $z = a$.

All of the setups use these same parameters: film thickness $2a = 60\,\text{nm}$, frequency $\omega = 3 \cdot 10^{15}\,\text{rad} \cdot \text{s}^{-1}$, plasma frequency for gold $\omega_p = 1.37 \cdot 10^{16}\,\text{rad} \cdot \text{s}^{-1}$, scaling amplitude of $A = 1.5 \cdot 10^4\ \text{V} \cdot \text{m}^{-1}$ and distance from the center of $r = 27\,\mu\text{m}$. On the right side of each interference pattern there is an image, which represents the nanostructure from which the SPPs were excited.

We start by constructing a SPID with square symmetry. It is clear, that in this model we see a form of a standing wave made as a sum of four contributions from each SPP source. Analogously, triangular (equilateral triangle) and hexagonal SPIDs are created.

Lastly, we will discuss the possibility of shifting individual sources slightly away from their original position in the distance r. As we can see in Fig. 2.6, by moving two opposite sources of the hexagon further from the center, we can achieve a distinct interference pattern, unlike the previous pattern with hexagonal symmetry (Fig. 2.5). In this case, the two opposite sources were moved from their previous distance of r to $1.05r$. All sorts of different on-demand patterns can be produced using this method.

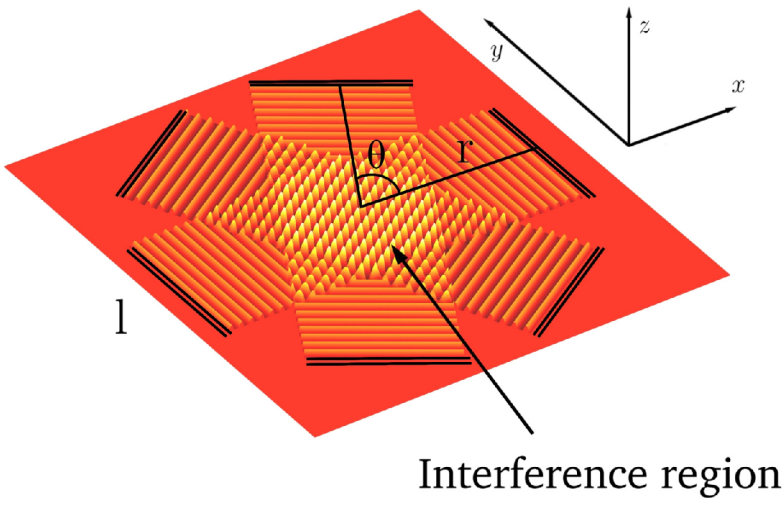

Figure 2.2: Function of the interference model in hexagonal geometry.

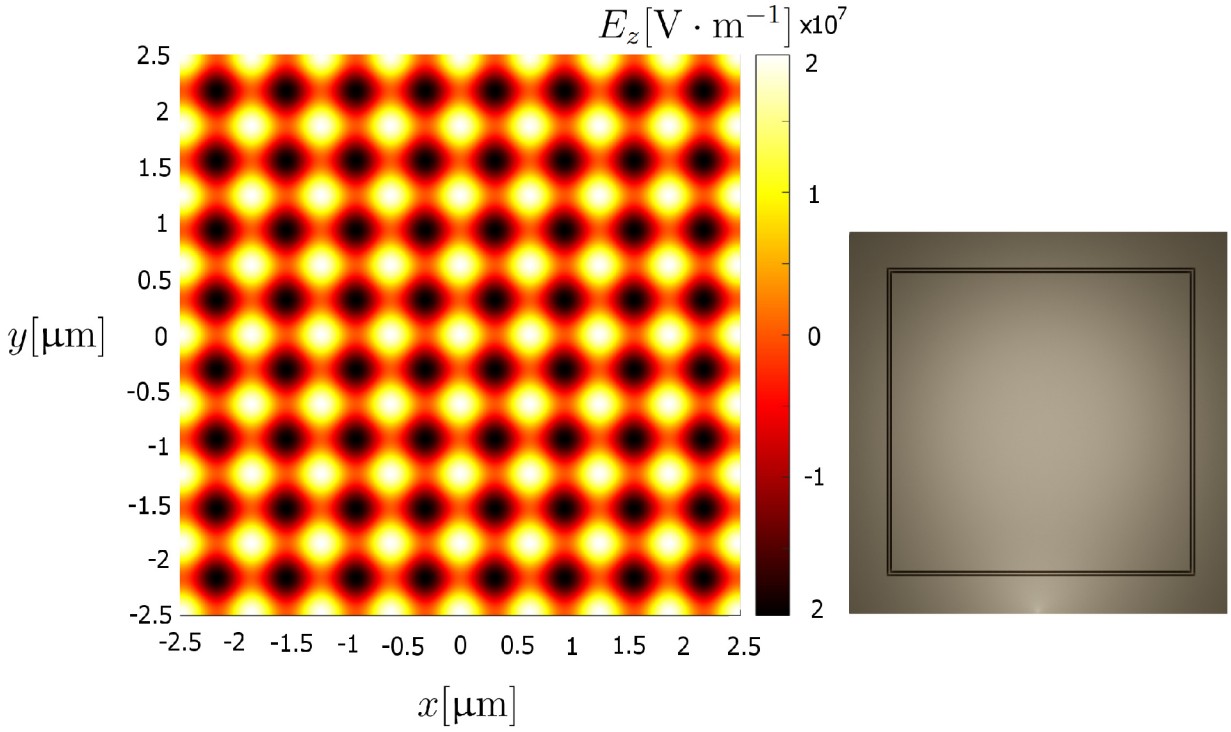

Figure 2.3: $E_{z,\mathrm{tot}}$ component of SPP. Interference in square symmetry.

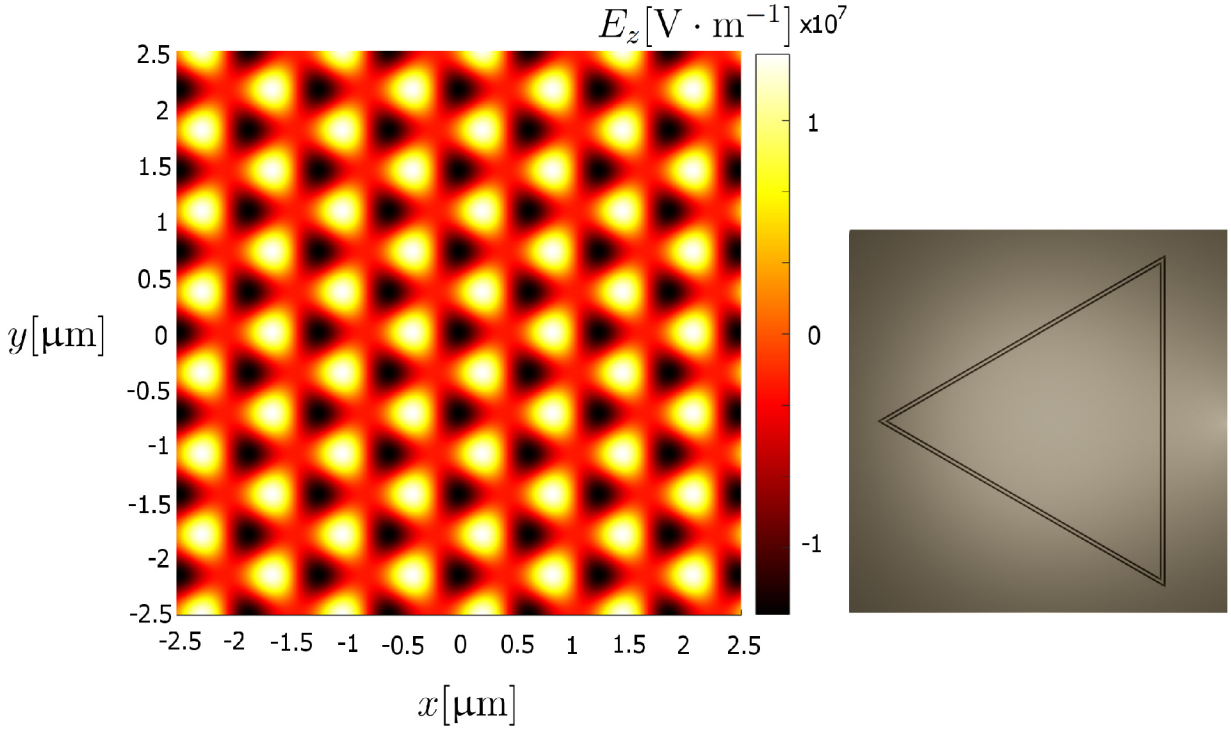

Figure 2.4: $E_{z,\mathrm{tot}}$ component of SPP. Interference in symmetry of equilateral triangle.

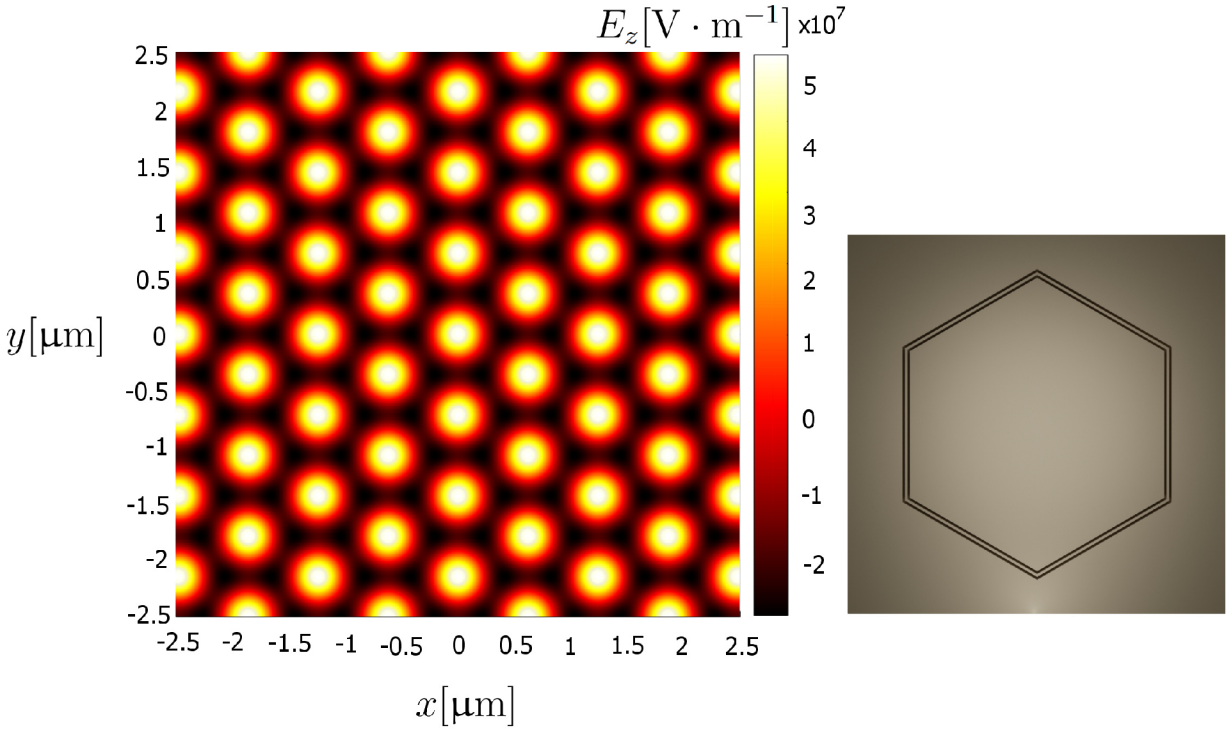

Figure 2.5: $E_{z,\mathrm{tot}}$ component of SPP. Interference in hexagonal symmetry.

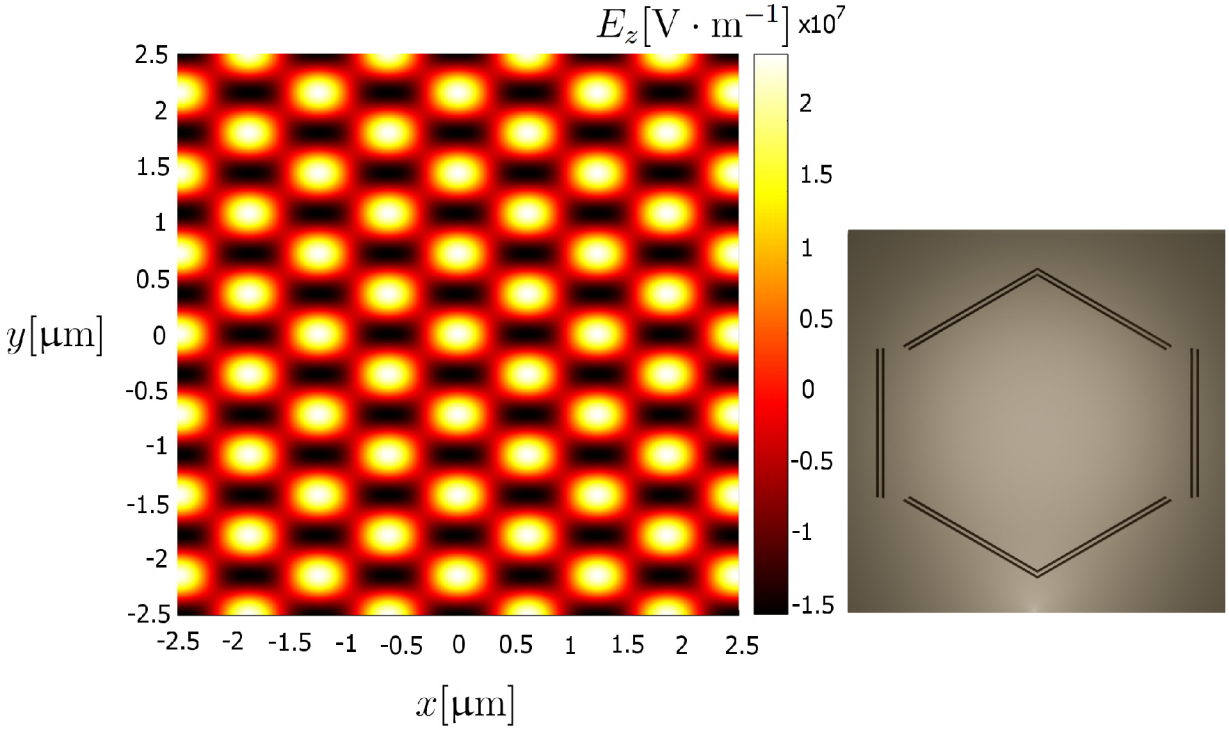

Figure 2.6: $E_{z,\mathrm{tot}}$ component of SPP. Interference in hexagonal symmetry with shifted sources.

3. Electron beam shaping

3.1. Electron-photon interaction

To shape an electron beam means to modulate its amplitude and alternate its phase via electron-photon interaction, which in inelastic interaction consists of gaining or losing quanta of energy in traversing through the optical field. In Fig. 3.1 elastic and inelastic interactions are depicted. In traversing through near-field the electron may undergo multiple of these interactions each with some probability, which will be discussed later in 3.2.2.

Electron-photon coupling via interaction has many potential applications, one of which is in the technique called photon-induced near-field electron microscopy. In this thesis, the focus is targeted on exploiting electron-photon interaction features in creating tailored electron beams (SEBs).

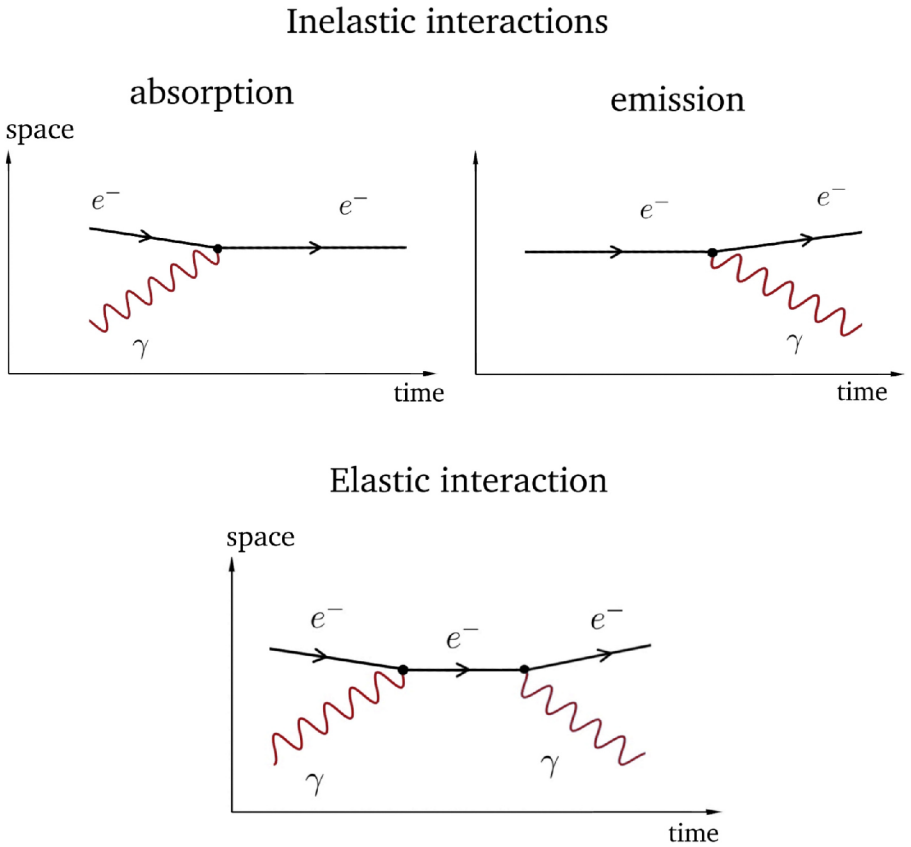

Figure 3.1: Electron-photon interaction both elastic and inelastic, depicted in Feynman diagrams [7], e^- as an electron and γ as a photon. Portrayed inelastic interactions results in the electron gaining (absorption) or losing (emission) a quantum of light energy $\hbar\omega$.

3.1.1. Free electron wave function

Before describing the evolution of an electron wave function in an optical field, we start with a wave function ψ of an electron in free space. Such wave function must be a solution of a Schrödinger equation:

$$\hat{\mathbf{H}}_0\psi(\mathbf{r},t) = \mathrm{i}\hbar\frac{\partial}{\partial t}\psi(\mathbf{r},t), \tag{3.1}$$

where $\mathbf{r}$ is space vector, $\hat{\mathbf{H}}_0 = -(\hbar^2/(2m_\mathrm{e}))\nabla^2$ is free space Hamiltonian, $\hbar$ reduced Planck's constant and m_e the mass of the electron.

The solution of Eq. (3.1) would be in a form of a plane wave, but such wave function would not be normalizable, due to the Heisenberg uncertainty principle. It is thus required to describe electron wave function as a wavepacket with normalizable envelope function $\mathbf{g}$, wavevector $\mathbf{q}_0$ and ω_e is its angular frequency:

$$\psi(\mathbf{r},t) = \mathbf{g}(\mathbf{r},t)\mathrm{e}^{-\mathrm{i}(\omega_\mathrm{e}t-\mathbf{q}_0\cdot\mathbf{r})}. \tag{3.2}$$

3.1.2. Interaction Hamiltonian

The following sections use theoretical background and relations, that come mostly from Refs. [19, 25, 11, 8, 26, 21]. We implement the interaction Hamiltonian into the Schrödinger equation, which will be enriched by a term for electron-photon interaction. Previous Schrödinger equation (3.1) is modified into:

$$\hat{\mathbf{H}}\psi(\mathbf{r},t) = \mathrm{i}\hbar\frac{\partial}{\partial t}\psi(\mathbf{r},t), \tag{3.3}$$

where the Hamiltonian $\hat{\mathbf{H}}$ for $(\nabla\cdot\mathbf{A}) = 0$, can be expressed as:

$$\hat{\mathbf{H}} = \frac{1}{2m_\mathrm{e}}(-\mathrm{i}\hbar\nabla - q\mathbf{A})^2 + q\varphi = -\frac{\hbar^2}{2m_\mathrm{e}}\nabla^2 + \frac{\mathrm{i}q\hbar}{m_\mathrm{e}}\mathbf{A}\cdot\nabla + \frac{q^2A^2}{2m_\mathrm{e}} + q\varphi, \tag{3.4}$$

where $\mathbf{A}$ is optical vector potential, φ scalar potential and q is in our case elementary charge $q = -e$. The Hamiltonian (3.4) can be divided into free space Hamiltonian $\hat{\mathbf{H}}_0$ from (3.1) and interaction Hamiltonian $\hat{\mathbf{H}}_1$ as $\hat{\mathbf{H}} = \hat{\mathbf{H}}_0 + \hat{\mathbf{H}}_1$. $\hat{\mathbf{H}}_1$ can furthermore be simplified using the Weyl (temporal) gauge ($A^0 = \varphi = 0$) and by neglecting the term $q^2A^2/(2m_\mathrm{e})$ since when considering the interaction of electrons with an optical near field, it is much smaller than other contributions and it becomes

$$\hat{\mathbf{H}}_1 = -\frac{\mathrm{i}e\hbar}{m_\mathrm{e}}\mathbf{A}\cdot\nabla. \tag{3.5}$$

To further simplify our problem, we will assume the interaction with monochromatic light with a well-defined frequency ω. Vector potential can then be approximated as [26]

$$\mathbf{A} \approx \frac{1}{\mathrm{i}\omega}\mathbf{E}\mathrm{e}^{-\mathrm{i}\omega t} - \frac{1}{\mathrm{i}\omega}\mathbf{E}^*\mathrm{e}^{\mathrm{i}\omega t}, \tag{3.6}$$

where * denotes a complex conjugate. By inserting Eq. (3.6) to Eq. (3.5) we get following form of the Hamiltonian:

$$\hat{\mathbf{H}}_1 = -\frac{e\hbar}{m_e\omega}\left(e^{-i\omega t}\mathbf{E}\cdot\nabla - e^{i\omega t}\mathbf{E}^*\cdot\nabla\right). \tag{3.7}$$

3.1.3. Modified electron wave function

In our geometry the electron moves along the z axis hence we can express momentum $\hbar\mathbf{q}_0 = (0,0,\hbar q_0)$, $\hbar q_0 = \sqrt{2m_eE_0}\sqrt{1+E_0/(2m_ec^2)}$ and electron kinetic energies to be narrowly spread and peaked around energy E_0. Eigen-energies of narrowly distributed wavevectors $\mathbf{q}$ in free space satisfy:

$$\hat{\mathbf{H}}_0 e^{i\mathbf{q}\cdot\mathbf{r}} = E_\mathbf{q} e^{i\mathbf{q}\cdot\mathbf{r}}. \tag{3.8}$$

$E_\mathbf{q}$ can be approximated $E_\mathbf{q} \approx E_0 + \hbar v(q_z - q_0)$, where $v = (\hbar q_0/m_e)(1+E_0/(m_ec^2))$ is the electron velocity, relativistically corrected due to the ultra-fast regime. Energy exchanges between the electron and light can only happen by transmitting quanta of energy i.e. in multiples of $\hbar\omega$. The wave function has now different energy distribution around $E_0 + \ell'\hbar\omega$. We also state $H_0 \approx E_0 - \hbar v(q_z - q_0)$. Because of the geometry involved, where the beam is parallel to z axis, we state $\nabla \to \frac{\partial}{\partial z}$. Under these approximations electron wave function may consist of two parts for fast evolving wave function of central momentum $\mathbf{q}_0$ and slowly evolving ϕ:

$$\psi(\mathbf{r},t) = e^{i(q_0z - E_0t/\hbar)}\phi(\mathbf{r},t) \tag{3.9}$$

Plugging Eq. (3.9) in Eq. (3.3), and considering Eq. (3.7) with the approximation stated above yields:

$$-\frac{ev}{\hbar\omega}\left(e^{-i\omega t}E_z - e^{i\omega t}E_z^*\right)\phi = \left(v\frac{\partial}{\partial z} + \frac{\partial}{\partial t}\right)\phi. \tag{3.10}$$

Solution for Eq. (3.10) is not as straightforward (obtained from [26],[11]), with $\mathbf{v} = (0,0,v)$:

$$\phi(\mathbf{r},t) = \phi_0(\mathbf{r}-\mathbf{v}t)e^{-\mathfrak{B}+\mathfrak{B}^*}, \tag{3.11}$$

where ϕ_0 is an initial state of the wave function before the interaction and $\mathfrak{B}$ is

$$\mathfrak{B}(\mathbf{r},t) = \frac{e\mathbf{v}}{\hbar\omega}\int_{-\infty}^{t} dt'\mathbf{E}(\mathbf{r}+\mathbf{v}t'-\mathbf{v}t,t')e^{-i\omega t'}. \tag{3.12}$$

For field $\mathbf{E}(x,y,z)$ changing in time insignificantly over the course of the interaction for slowly evolving ϕ, thus is a function only of $(\mathbf{r})$, it is possible to rewrite $\mathfrak{B}$ as:

$$\mathfrak{B}(\mathbf{r},t) = \beta(\mathbf{r})\mathrm{e}^{\mathrm{i}\omega(z/v-t)}, \tag{3.13}$$

where

$$\beta(\mathbf{r}) = \frac{e}{\hbar\omega}\int_{-\infty}^{z} dz^{'} E_{z^{'}}(x,y,z^{'})\mathrm{e}^{-\mathrm{i}\omega z^{'}/v}. \tag{3.14}$$

Using Jacobi-Anger expansion $\mathrm{e}^{\mathrm{i}u\sin\theta} = \sum_{n=-\infty}^{\infty} J_n(u)\mathrm{e}^{\mathrm{i}n\theta}$ for function $\mathrm{e}^{-\mathfrak{B}+\mathfrak{B}^*}$ (Appendix 3.3.2) yields:

$$\mathrm{e}^{-\mathfrak{B}+\mathfrak{B}^*} = \sum_{\ell} J_\ell(2|\mathfrak{B}|)\mathrm{e}^{\mathrm{i}\ell\arg(-\mathfrak{B})}, \tag{3.15}$$

which furthermore after substitution of Eq. (3.13) equals to

$$\sum_{\ell} J_\ell(2|\beta|)\mathrm{e}^{\mathrm{i}\ell\arg(-\beta)}\mathrm{e}^{\mathrm{i}\ell\omega(z/v-t)}, \tag{3.16}$$

where J_ℓ are first kind Bessel functions of ℓ-th order and $\arg(-\beta)$ is argument of complex number $-\beta$.
For simplicity we can confine β-dependent terms from (3.16) into coefficient

$$f_\ell(\beta) = J_\ell(2|\beta|)\mathrm{e}^{\mathrm{i}\ell\arg(-\beta)} \tag{3.17}$$

and with f_ℓ the Eq. (3.11) transforms to

$$\phi(\mathbf{r},t) = \phi_0(\mathbf{r}-\mathbf{v}t)\sum_{\ell}\mathrm{e}^{\mathrm{i}\ell\omega(z/v-t)}f_\ell(\beta(\mathbf{r})). \tag{3.18}$$

Eq. (3.18) will be a crucial element of the description of shaped electron beams created via the interaction with plasmonic near-fields. The implementation into the model involves both electron wave function and surface plasmon polaritons and will be discussed in the next portion of the thesis.

3.2. Implementation

3.2.1. β coefficient

Now we combine the theory of near-fields and electron-photon interaction. The plasmonic interference gives forms of electric fields confined at the thin film, which defines an interaction volume for the electron-photon interaction. Since the electric is evanescent in the z direction, the interaction volume is defined with respect to this exponential decay.

The integral in (3.14) will converge in $-\infty$ and ∞. In reality, however, has finite limits $-z_{min}, z_{max}$ due to the space limitation of the experiments. With XY plane they define an effective interaction volume$x \times y \times (z_{min} + z_{max})$ as shown in Fig 3.2. But data from the model show that E_z decays rapidly in short distances (compared to electron trajectory) perpendicular to the film. In the limits, E_z decays to zero, it therefore has zero contribution to β. We can thus count with the argument of the integral in $-z_{min}$, z_{max} as zero.

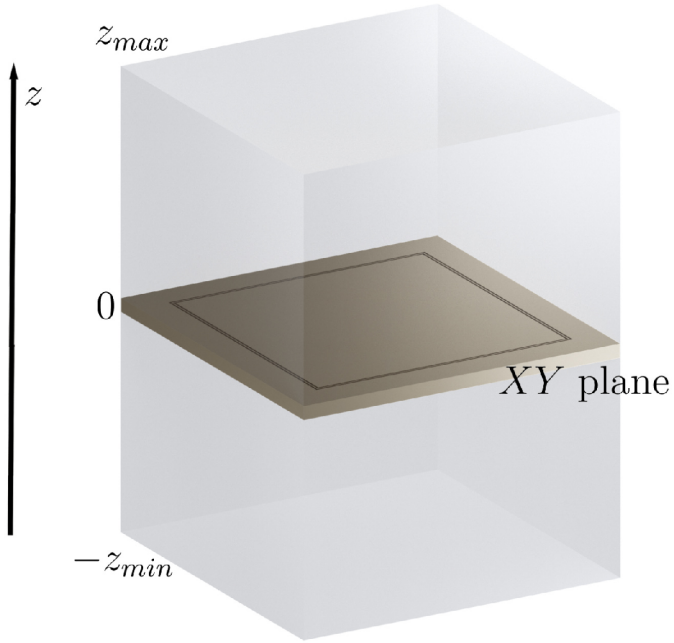

Figure 3.2: Interaction volume defined as $x \times y \times (z_{min} + z_{max})$

The integral in (3.14) is, in this approximation, no longer dependent on z; hence $\beta(x, y)$ is a function of x, y only, and it is possible to evaluate its value for each point in XY plane. We take electric fields from Eqs. (2.1)-(2.3). And divide contributions to β into three regions (III, I, II), correspondingly to the expressions for the electric field in these regions.

The total $\beta(x,y)$ consists of contributions of a sum of all three regions as well as a sum of interfered fields (2.4). $R_{\pm lim}$ are denoting integration limits for each region R. We also use previously defined x_j, y_j from (2.4) and corresponding wavevectors.

$$\beta(x,y) = \frac{e}{\hbar\omega}\sum_{R}\sum_{\text{source } j}\int_{R_{-lim}}^{R_{+lim}} dz^{'} E^{R}_{z,j}(x_j, y_j, z^{'})\mathrm{e}^{-\mathrm{i}\omega z^{'}/v}, \tag{3.19}$$

where β^R for each region R and source j is:

$$\beta^{III}_{j}(x,y) = \frac{e}{\hbar\omega}\int_{a}^{z_{max}} dz^{'}(-A)\frac{K}{\omega\varepsilon_0\varepsilon_3}\mathrm{e}^{\mathrm{i}(k_{x,j}x_j+k_{y,j}y_j)}\mathrm{e}^{-\alpha_3 z^{'}}\mathrm{e}^{-\mathrm{i}\omega z^{'}/v}, \tag{3.20}$$

$$\beta^{I}_{j}(x,y) = \frac{e}{\hbar\omega}\int_{-a}^{a} dz^{'}\left(C\mathrm{e}^{\alpha_1 z^{'}} + D\mathrm{e}^{-\alpha_1 z^{'}}\right)\frac{K}{\omega\varepsilon_0\varepsilon_1}\mathrm{e}^{\mathrm{i}(k_{x,j}x_j+k_{y,j}y_j)}\mathrm{e}^{-\mathrm{i}\omega z^{'}/v}, \tag{3.21}$$

$$\beta^{II}_{j}(x,y) = \frac{e}{\hbar\omega}\int_{-z_{min}}^{-a} dz^{'}(-B)\frac{K}{\omega\varepsilon_0\varepsilon_2}\mathrm{e}^{\mathrm{i}(k_{x,j}x_j+k_{y,j}y_j)}\mathrm{e}^{\alpha_2 z^{'}}\mathrm{e}^{-\mathrm{i}\omega z^{'}/v}. \tag{3.22}$$

With the assumption of integral argument value in $-z_{min}$, z_{max} as 0. (3.20)-(3.22) can be evaluated as

$$\beta^{III}_{j}(x,y) = -A\frac{e}{\hbar\omega^2}\frac{K}{\varepsilon_0\varepsilon_3(\alpha_3+\mathrm{i}\omega/v)}\mathrm{e}^{\mathrm{i}(k_{x,j}x_j+k_{y,j}y_j)}\mathrm{e}^{-a(\alpha_3+\mathrm{i}\omega/v)}, \tag{3.23}$$

$$\beta^{I}_{j}(x,y) = \frac{e}{\hbar\omega^2}\frac{K\mathrm{e}^{\mathrm{i}(k_{x,j}x_j+k_{y,j}y_j)}}{\varepsilon_0\varepsilon_1}\left(C\frac{\mathrm{e}^{a(\alpha_1-\mathrm{i}\omega/v)}-\mathrm{e}^{-a(\alpha_1-\mathrm{i}\omega/v)}}{\alpha_1-\mathrm{i}\omega/v} + D\frac{\mathrm{e}^{-a(\alpha_1+\mathrm{i}\omega/v)}-\mathrm{e}^{a(\alpha_1+\mathrm{i}\omega/v)}}{-\alpha_1-\mathrm{i}\omega/v}\right), \tag{3.24}$$

$$\beta^{II}_{j}(x,y) = -B\frac{e}{\hbar\omega^2}\frac{K}{\varepsilon_0\varepsilon_2(\alpha_2-\mathrm{i}\omega/v)}\mathrm{e}^{\mathrm{i}(k_{x,j}x_j+k_{y,j}y_j)}\mathrm{e}^{-a(\alpha_2-\mathrm{i}\omega/v)}. \tag{3.25}$$

The sum of integrals from (3.19), after the evaluation of the integrals, transforms into a sum over (3.23)-(3.25):

$$\beta(x,y) = \sum_{R}\sum_{\text{source } j}\beta^{R}_{j} \tag{3.26}$$

3.2.2. f_ℓ dependence

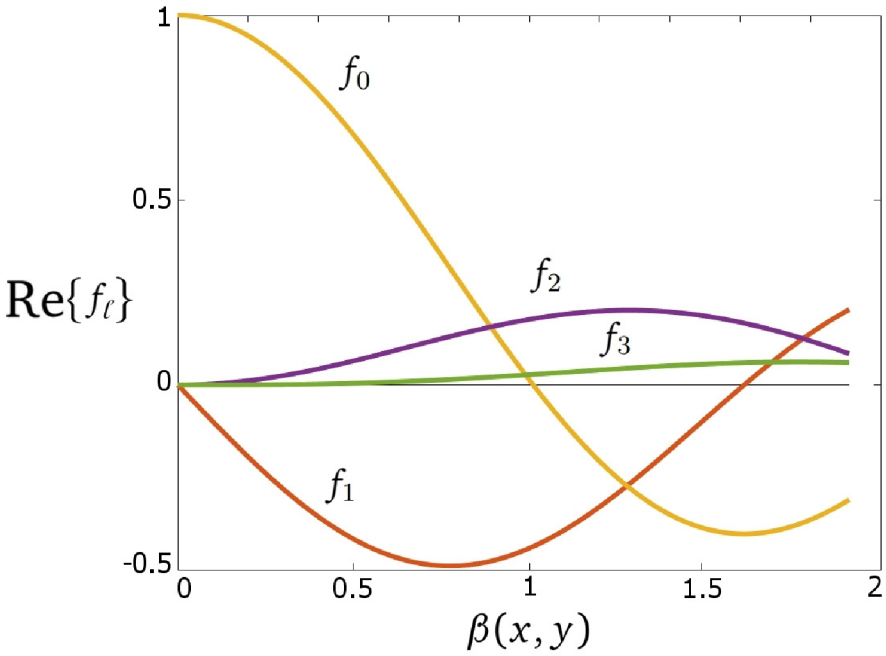

Figure 3.3: Bessel dependence of Re$\{f_\ell\}$ in a random point $[x, y]$. Bear in mind that these graphs change along x, y. β is generally complex and can even be negative, but it always shows Bessel dependence.

Since $\beta(x, y)$ does not depend on z, $f_\ell(\beta(x, y))$ does not depend on z either, and it thus only changes in the XY plane. $\sum_\ell e^{i\ell\omega(z/v-t)} f_\ell(\beta(\mathbf{r}))$ in Eq. (3.18) give an x, y dependent 2D map of the interaction for specific z and time t. If we take a closer look at

$$f_\ell(\beta) = J_\ell(2|\beta|)e^{i\ell \arg(-\beta)},$$

we find that its magnitude for every ℓ is following first kind Bessel function of ℓ-th order. ℓ represents the number of quanta electron has received via the interactions, and $|f_\ell(\beta)|^2$ acts like a probability of electron gaining energy $\ell\hbar\omega$. Moreover, for the probability of the sum of all orders, we have:

$$\sum_\ell |f_\ell(\beta)|^2 = 1. \tag{3.27}$$

Because electrons will have different energies after the electron-photon interaction, it is suitable to use EELS (electron energy-loss spectroscopy) to study energy distribution of the electrons in the beam. Some interesting features of electron energy distribution may occur due to the Bessel-function dependence. As we see in Fig. 3.3, if $\beta \to 0$, the highest contribution comes from f_0, that means almost no interaction was involved at $\beta \to 0$, that is due to the very weak electric field involved; therefore almost no interaction comes into play, and electrons pass through the interaction volume undisturbed. As we move towards higher values of β, other contributions

play a more significant role. Especially in the section where the value of f_0 starts approaching zero, we see that f_1 is significant, which means that within this configuration of factors defining this particular β, we would detect a high percentage of electrons with energy representing one photon energy quantum gain or loss.

Our interest will now transfer to variables that are affecting β and are inherently controlled by experimental setup, that is, a dependence on the intensity of the illumination, which is, in the case of the model, represented by scaling amplitude A. The next variable is the light energy, and lastly, electron speed v and the film thickness $2a$, which vary the outcome of the integrals in Eq. (3.19).

In terms of thickness, we try to use film as thin as possible. Otherwise, the electron beam could be heavily affected by interaction with the bulk of the metal. In ultra-fast electron regime and thin film (tens of nm), we assume a minor influence of the bulk. The easiest one of the variables to change is the light intensity. The energy of the photons is also easy to control. The limitations we might have is using light of very high frequencies, that is X-ray regime, with hard-to-get sources. The experimental setup would also have to be adjusted due to safety reasons.

Figs. 3.4 and 3.5 show the dependence of f_0, f_1 on light energy and amplitude A representing light intensity. Implicitly expressed intensity is not used, because every setup (Figs. 2.3-2.6) and interference results in different values of intensity. Scaling amplitude A, on the other hand, is set in the computation and very easily adjustable to correspond to experimental data, hence it is used instead.

For low energies of light, we see fast-changing f_0, f_1 when moving towards high intensities. This behavior is very sensitive to slight changes in the setup and, therefore, not very suitable for experiments. It is thus appropriate to stay above 1 eV, corresponding to wavelength $\lambda = 1240$ nm (near-infrared regime). In the model will we use light from the visible spectrum.

3.2.3. Contrast function

Contributions of f_ℓ of higher order $|\ell| > 0$ will result in higher probabilities of interaction and have an effect on the so-called contrast function, which is a relation between the maximum and minimum peaks of the electron wave, we can define contrast function as:

$$C = \frac{F_{\max} - F_{\min}}{F_{\max} + F_{\min}}, \tag{3.28}$$

We define $|\phi_0 \sum_\ell e^{i\ell\omega(z/v-t)} f_\ell(\beta(\mathbf{r}))|^2 = F(x, y, z, t)$ ranging within $\langle F_{\min}, F_{\max}\rangle$ in value, which we then insert in (3.28)

Contrast function plays an important role as a property of SEB and will represent the magnitude of wave function shaping i.e. high contrast means strong modification and vice versa.

This value is important because a certain situation may occur when we get the shaped beam after the interaction, but it might have insignificant contrast. Therefore, it would, in reality, be difficult to measure and analyze. We thus have to pay attention to the variables which affect the contrast. Those will be the same variables, which β depends on.

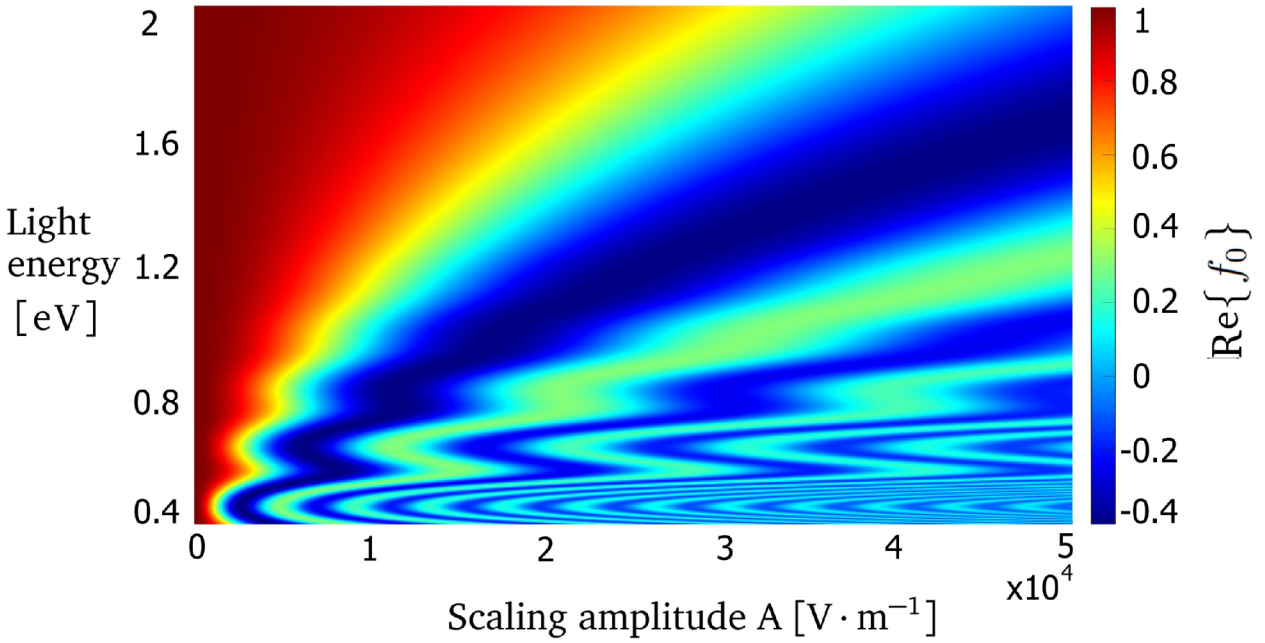

Figure 3.4: Real part of f_0 as a function of intensity represented by amplitude A and photon energy.

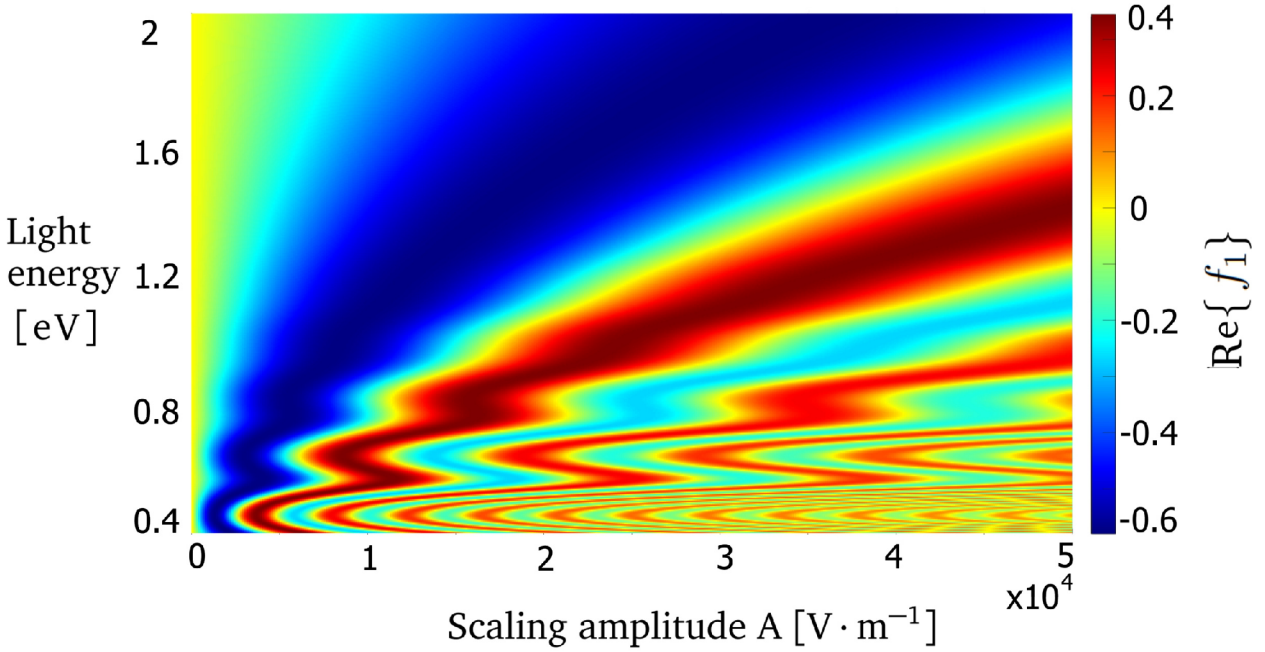

Figure 3.5: Real part of f_1 as a function of intensity represented by amplitude A and photon energy.

3.3. Resulting shaped electron beams

The process of creating SEBs is based on the theoretical description above. In the description and calculation of the shaped electron wave function, the starting point will be the previously derived Eq. (3.18).

For simplicity, we assume ϕ_0 is a constant representing a plane wave across the whole interaction volume and does not change its form due to diffraction, since the interaction length is small in comparison to distances from the electron source to the metal film. We bear in mind that ϕ_0 can be modified.

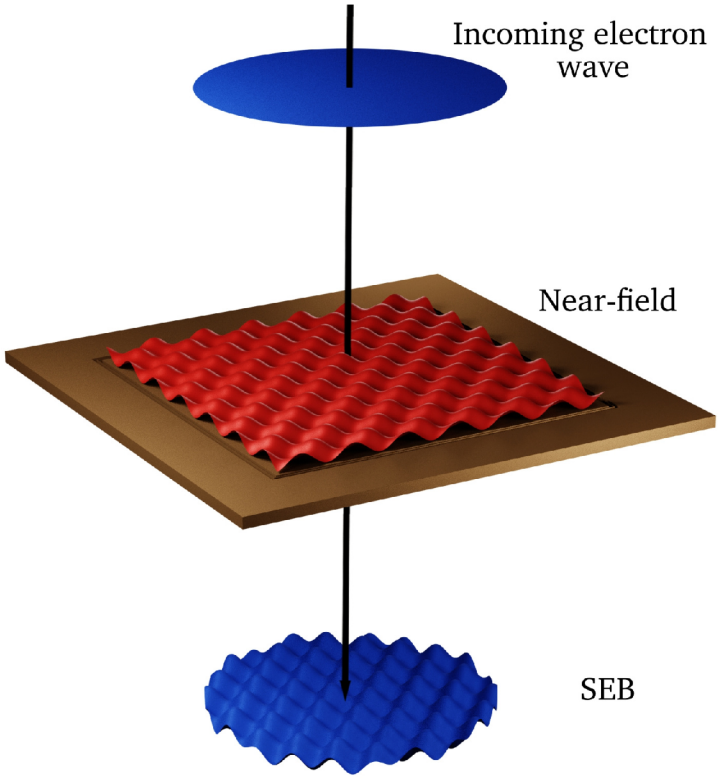

Figure 3.6: We see the arrangement of traversing electron wave. The trajectory of electrons is set parallel to z-axis, and we state that wave function $\phi(\mathbf{r}, t)$ changes only due to the electron-photon interaction and does not change its shape due to diffraction across the interaction volume.

3.3.1. Amplitude modulation

Figs. 3.7-3.9 show results in the form of shaped electron beams in correspondence to interfered plasmonic near field 2.3-2.6. We set the time as $t = 0$ after the electron leaves the interaction volume and will no longer interact, that is the point where we display the wave function. We, therefore, do not inspect the change in z. Electron velocity is $v = 0.778c$, which is an electron with 300 keV of kinetic energy. Metal film thickness $2a = 60$ nm. Used metal is gold with plasma frequency $\omega_p = 1.37 \cdot 10^{16}\,\mathrm{rad} \cdot \mathrm{s}^{-1}$. Sources in $r = 27\,\mu\mathrm{m}$ illuminated by light with

frequency $\omega = 3 \cdot 10^{15}\,\mathrm{rad} \cdot \mathrm{s}^{-1}$, which corresponds to energy of 1.95 eV. Scaling amplitude A and therefore the light intensity will be stated below each figure since we will later observe the effect the modification of amplitude A has. The plots show real and imaginary parts of $\phi(x, y, t = 0)$ in units of ϕ_0.

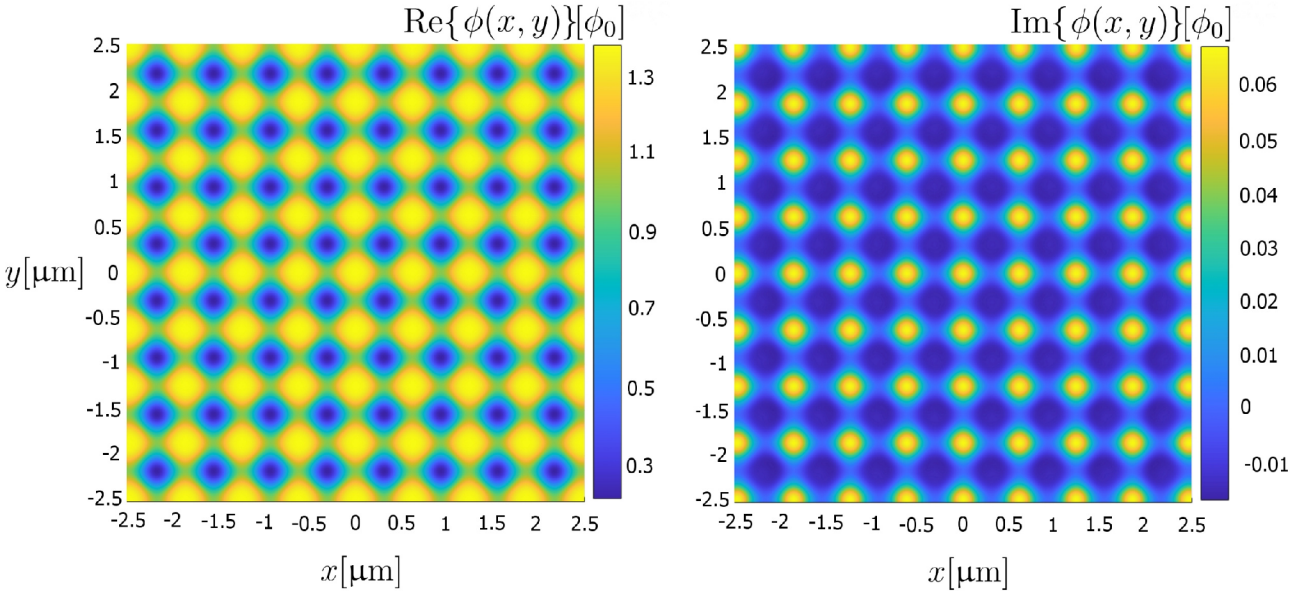

Figure 3.7: SEB created on square geometry SPID. Contrast $C = 0.947$, amplitude $A = 3 \cdot 10^4$ V · m^{-1} resulting in peak intensity $E_z = 4 \cdot 10^7$ V · m^{-1}

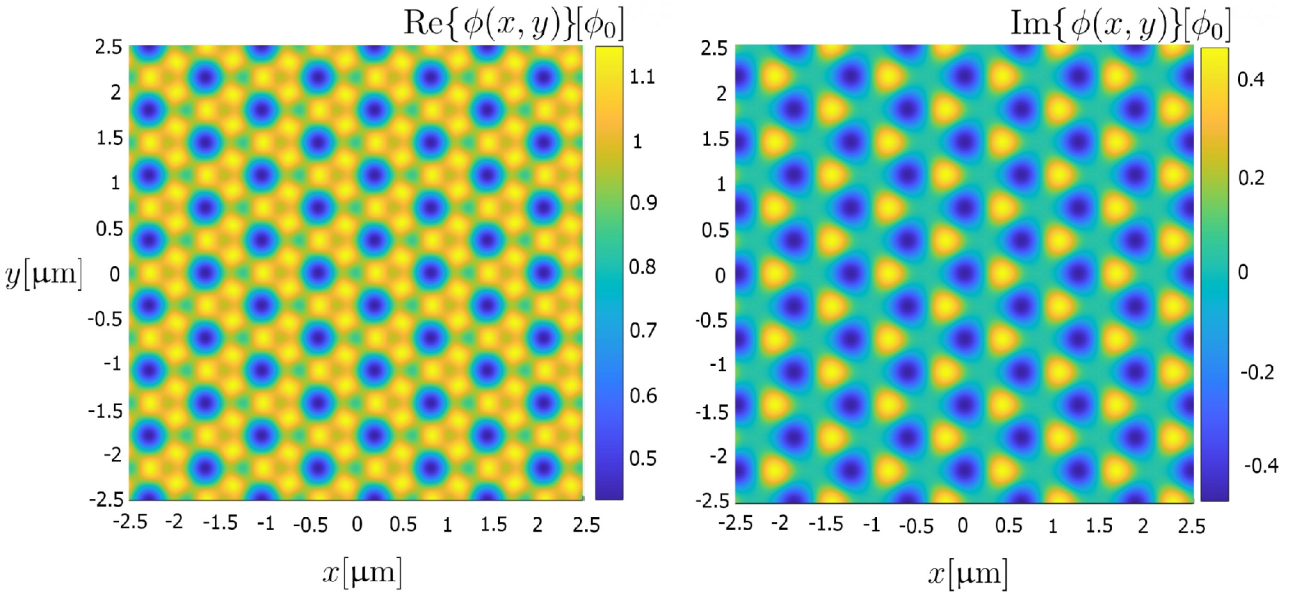

Figure 3.8: SEB created on equilateral triangle geometry SPID. Contrast $C = 0.763$, amplitude $A = 3 \cdot 10^4$ V · m^{-1} resulting in peak intensity $E_z = 3.3 \cdot 10^7$ V · m^{-1}

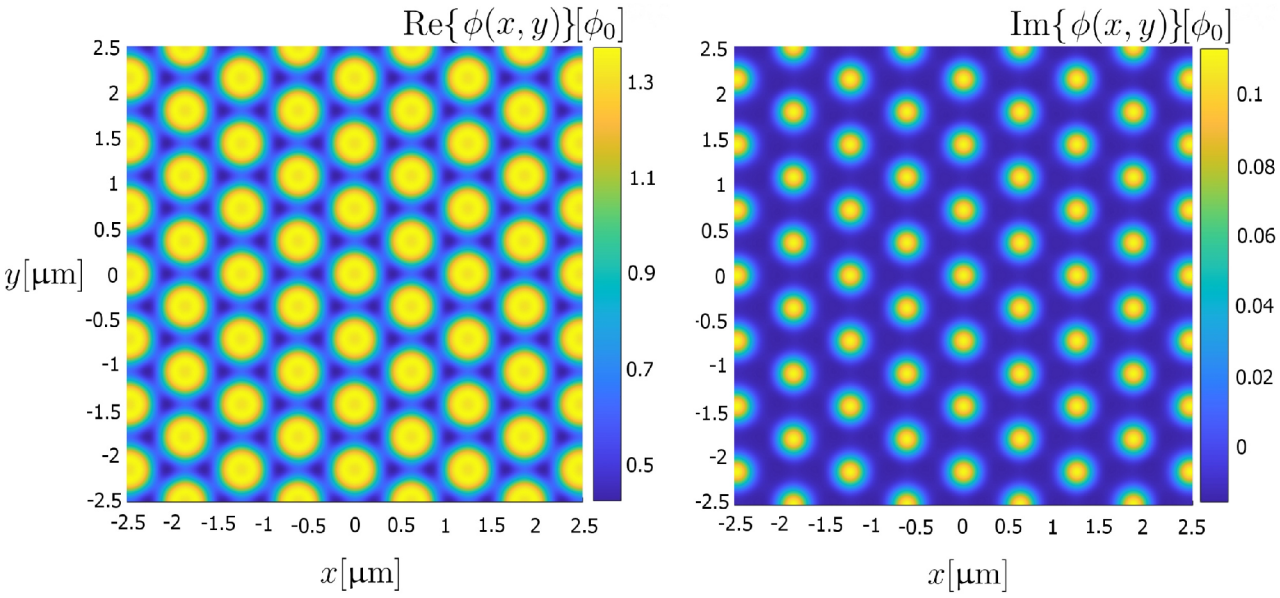

Figure 3.9: SEB created on hexagonal geometry SPID. Contrast $C = 0.828$, amplitude $A = 3 \cdot 10^4$ V$\cdot$m^{-1} resulting in peak intensity $E_z = 6 \cdot 10^7$ V$\cdot$m^{-1}

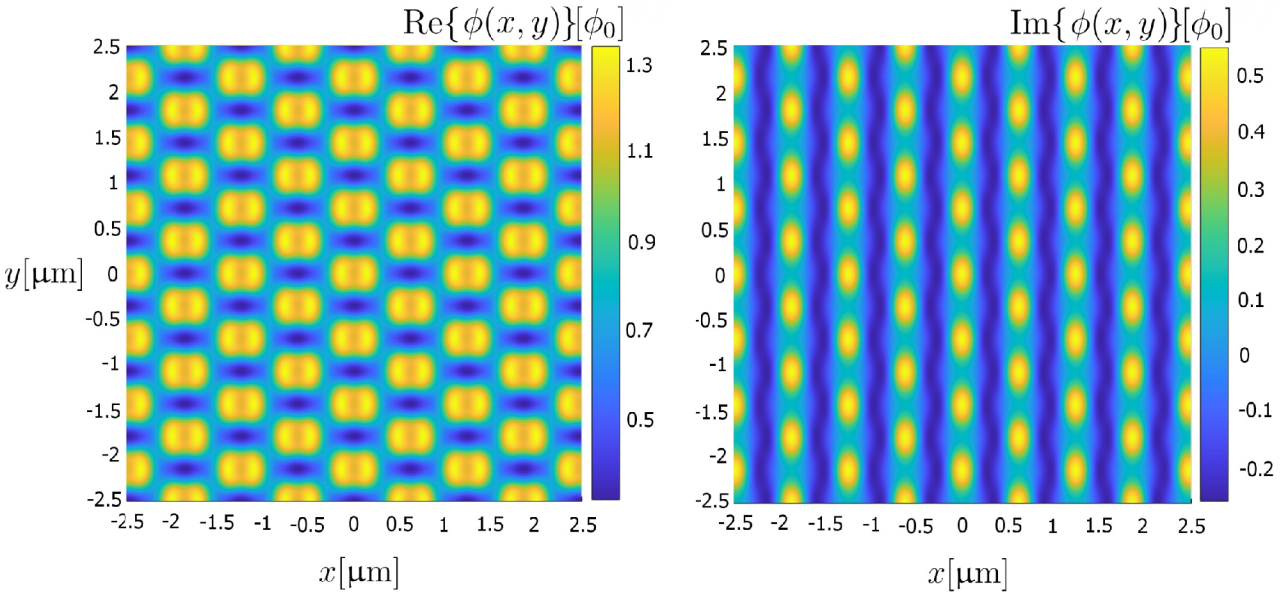

Figure 3.10: SEB created on hexagonal geometry SPID with shifted sources analogous to 2.6. Contrast $C = 0.880$, amplitude $A = 3 \cdot 10^4$ V$\cdot$m^{-1} resulting in peak intensity $E_z = 4.7 \cdot 10^7$ V$\cdot$m^{-1}

In Figs. 3.11, 3.12 SEB created on hexagonal geometry SPID has its ϕ decomposed into individual contributions from f_0 up to f_3, since those are the most influential, real parts of f_ℓ shown. Contrast of ϕ is $C = 0.828$, amplitude $A = 3 \cdot 10^4\ \mathrm{V \cdot m^{-1}}$ resulting in peak intensity $E_z = 6 \cdot 10^7\ \mathrm{V \cdot m^{-1}}$

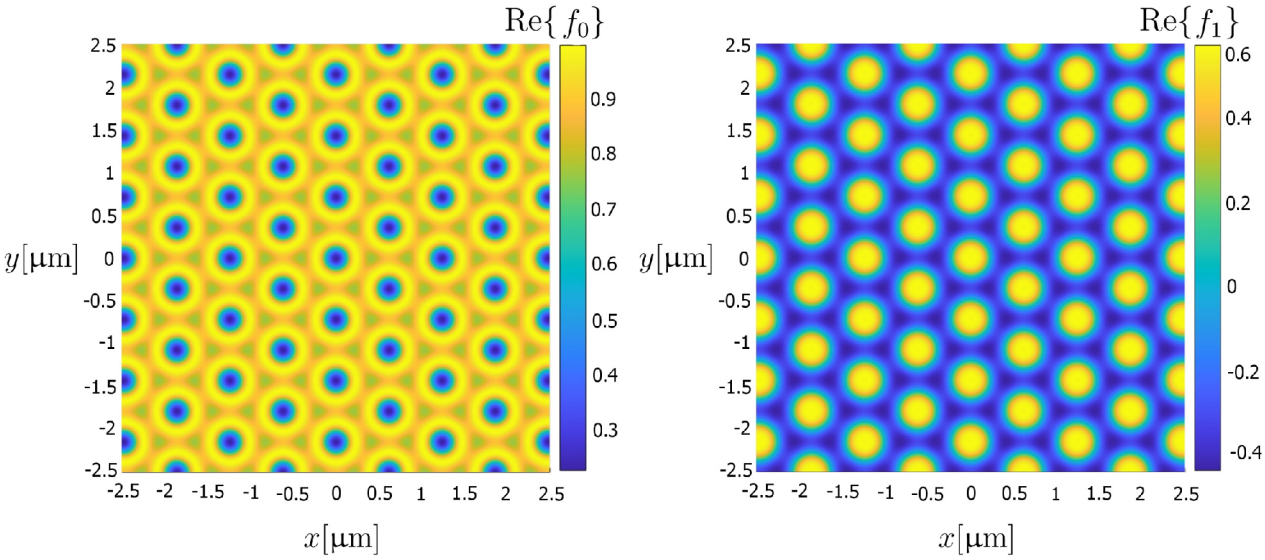

(a) f_0 contribution (b) f_1 contribution

Figure 3.11

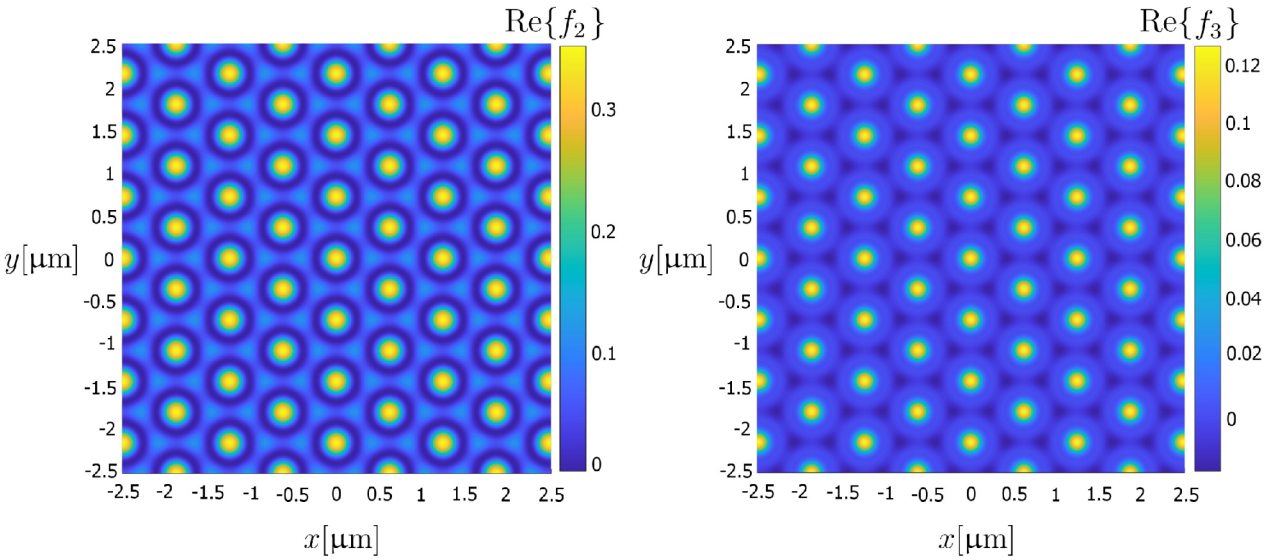

(a) f_2 contribution (b) f_3 contribution

Figure 3.12

In Figs. 3.13, 3.14 show SEBs created on hexagonal symmetry SPID, illuminated by different light intensities. It is apparent, that for higher intensities (and therefore β), orders of $|\ell| > 0$ gain in significance. We can see that with increasing light intensity contrast increases as well.

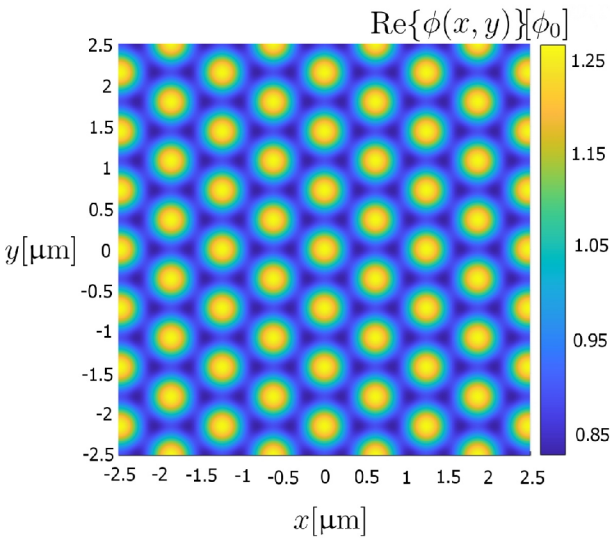

(a) Contrast $C = 0.408$
Amplitude $A = 1 \cdot 10^4\ \mathrm{V \cdot m^{-1}}$
Peak intensity $E_z = 2 \cdot 10^7\ \mathrm{V \cdot m^{-1}}$

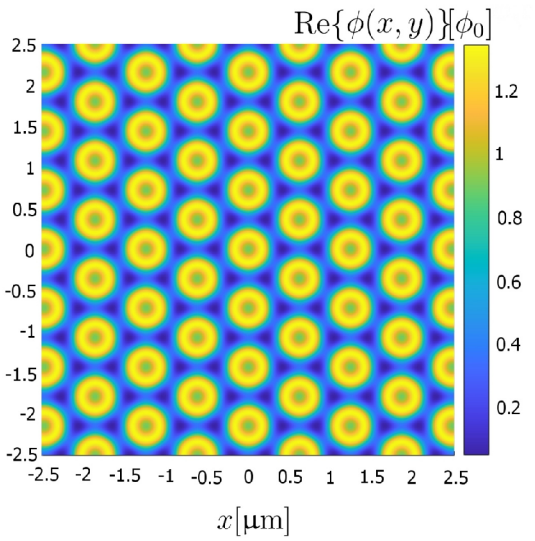

(b) Contrast $C = 0.997$
Amplitude $A = 5 \cdot 10^4\ \mathrm{V \cdot m^{-1}}$
Peak intensity $E_z = 10 \cdot 10^7\ \mathrm{V \cdot m^{-1}}$

Figure 3.13

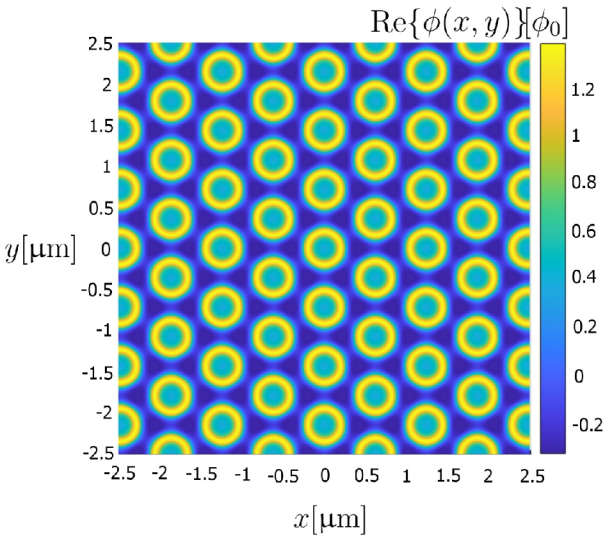

(a) Contrast $C = 0.999$
Amplitude $A = 10 \cdot 10^4\ \mathrm{V \cdot m^{-1}}$
Peak intensity $E_z = 20 \cdot 10^7\ \mathrm{V \cdot m^{-1}}$

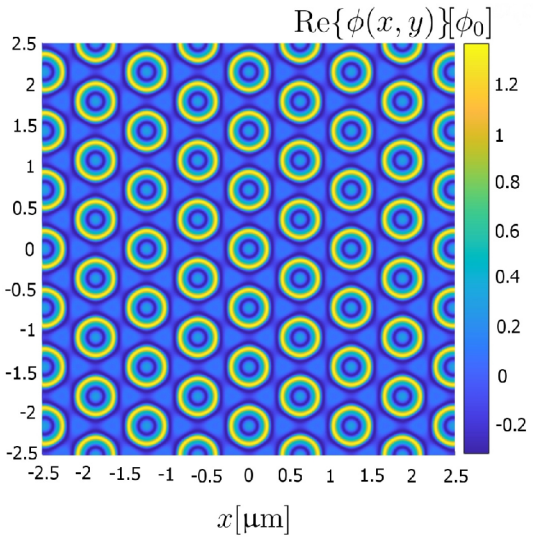

(b) Contrast $C = 1.00$
Amplitude $A = 20 \cdot 10^4\ \mathrm{V \cdot m^{-1}}$
Peak intensity $E_z = 40 \cdot 10^7\ \mathrm{V \cdot m^{-1}}$

Figure 3.14

3.3.2. Phase modulation

Now we take a closer look at the phase modulation of $\phi(x, y, t = 0)$. The change of phase is dependent on the β, thus also dependent on intensity. Same setup of constants $v, 2a, \omega_p, r, \omega$ as in 3.3.1 is used. Phases of ϕ from 3.13, 3.14 are displayed, i.e. for amplitudes mentioned below the figures. As we see in Figs. 3.15, 3.16, for lower intensities the phase falls in only small intervals, whereas high intensities result in phase modulation interval $\langle -\pi, \pi \rangle$.

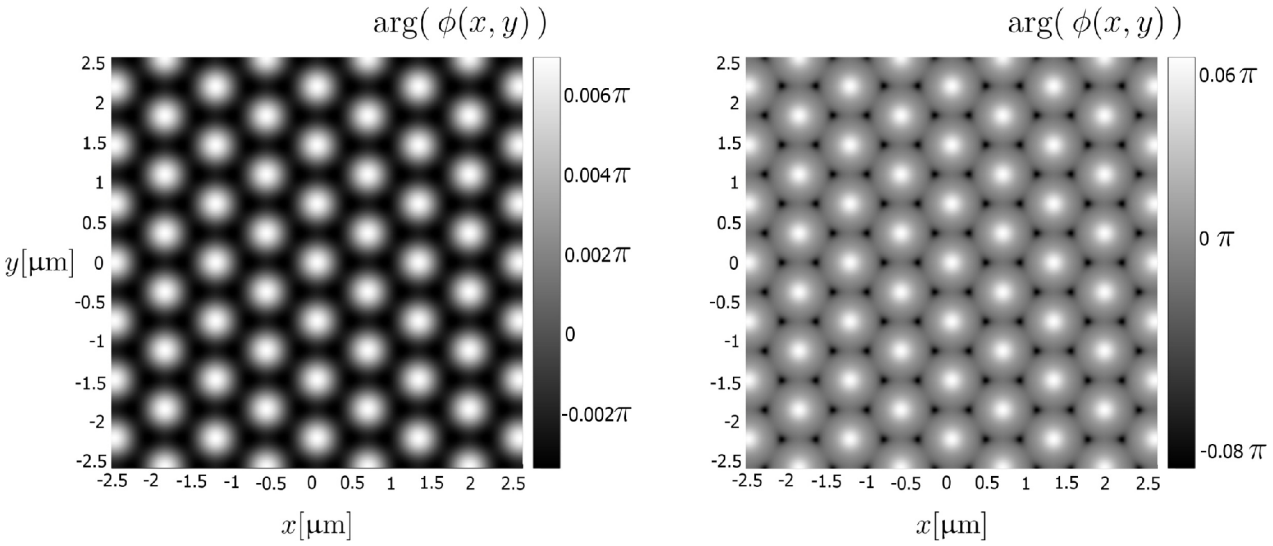

(a) $\phi(x, y)$ phase, peak intensity $E_z = 2 \cdot 10^7$ V · m^{-1} (b) $\phi(x, y)$ phase, peak intensity $E_z = 10 \cdot 10^7$ V · m^{-1}

Figure 3.15

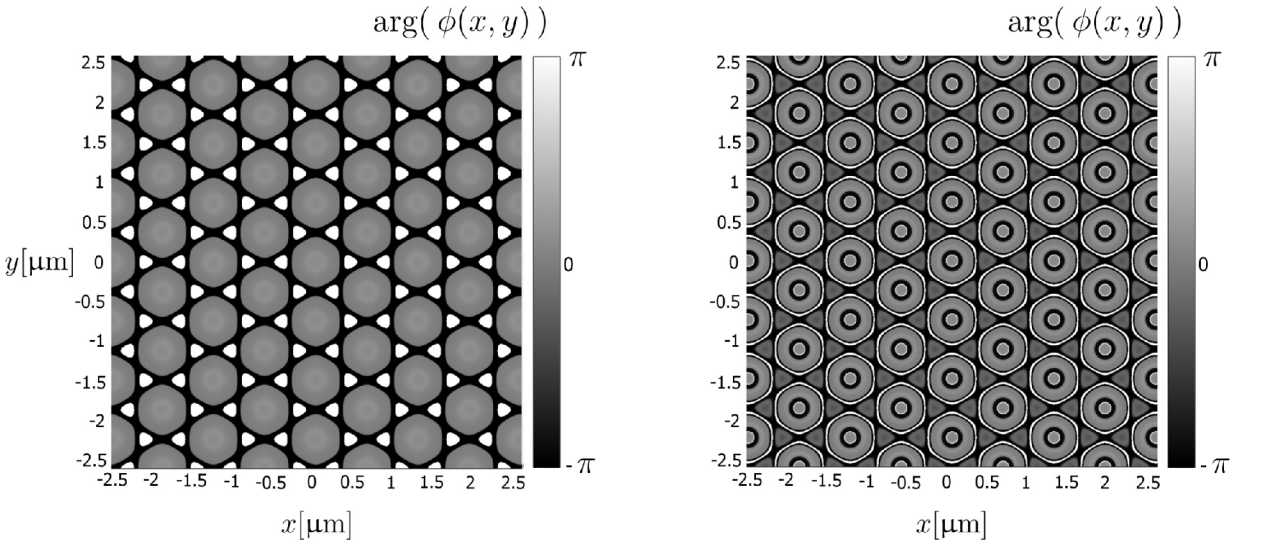

(a) $\phi(x, y)$ phase, peak intensity $E_z = 20 \cdot 10^7$ V · m^{-1} (b) $\phi(x, y)$ phase, peak intensity $E_z = 40 \cdot 10^7$ V · m^{-1}

Figure 3.16

SUMMARY

The thesis was focused on obtaining a theoretical description of shaped electron beams. SEBs are created via electron-photon interaction, where the photons are, in the case of this thesis, represented by plasmonic optical near-fields. In correspondence to the theory, an analytical model of the interaction was developed and used in depicting shaped electron wave functions. The model itself was designed and analyzed in MATLAB R2021b software environment.

The core subject of Chapter 1 was the general description of electromagnetic waves and the electromagnetic response of metals in the presence of optical fields. The response is represented by a dielectric function, which was obtained from the Drude model of free electrons. We discussed the possibility of bounding light to the metal-dielectric interface, which gives rise to surface plasmon polaritons. We described SPPs on one interface and then in the case of a thin metal film, where coupled modes of SPP occur. This chapter also involved the discussion about the conditions of SPP excitation.

In Chapter 2, we focused on the interference of SPPs on a thin metallic film. The surface plasmon interference device was modeled and gave us specific SPP interference patterns. These SPP patterns were later used as an example for SEB formation in 3.3.1.

The main matter of the thesis, the electron-photon interaction, was described in Chapter 3. We got the forms of the interaction Hamiltonian, which represents the interaction and then used it in the Schrödinger equation. That gave us the form of the electron wave function, which is dependent on the strength and shape of the E_z component of the SPPs. Then we discussed the properties of the wave function, which were confined in β coefficient. β has direct impact on $|f_\ell|^2$, the probability of electron gaining $\ell\hbar\omega$ of energy. These probabilities then determine the amplitude and phase modulation level as shown in sections 3.3.1 and 3.3.2, which show the final results of the model.

SEBs might have a wide variety of applications, although, to this day, not many experiments have been conducted. Therefore, this theoretical background, findings, and the model could have an important role in predicting the results of potential future experiments.

APPENDIX

TE - polarity

Here we show that SPPs cannot exist in TE polarity [20]: For TE polarity applies:

$$E_y^{II} = A_2 \mathrm{e}^{\mathrm{i}(k_x x - \omega t)} \mathrm{e}^{-\alpha_2 z}$$

$$E_y^{I} = A_1 \mathrm{e}^{\mathrm{i}(k_x x - \omega t)} \mathrm{e}^{\alpha_1 z}$$

$$H_x^{II} = -A_2 \frac{1}{\mu_0 \mathrm{i}\omega}(-\alpha_2) e^{\mathrm{i}(k_x x - \omega t)} \mathrm{e}^{-\alpha_2 z}$$

$$H_x^{I} = -A_1 \frac{1}{\mu_0 \mathrm{i}\omega}(\alpha_1) e^{\mathrm{i}(k_x x - \omega t)} \mathrm{e}^{\alpha_1 z}$$

If we use the boundary condition for continuity of E_y, which yields $A_1 = A_2$, and for continuity of H_x we see that with no free currents involved:

$$A_1(\alpha_1 + \alpha_2) = 0$$

That only has trivial solution $A_1 = 0$, since both $Re\{\alpha_1\} > 0$ and $Re\{\alpha_1\} > 0$, therefore SPPs do not exist in TE polarization.

Jacobi-Anger expansion

Jacobi-Anger expansion from `https://en.wikipedia.org/wiki/Jacobi%E2%80%93Anger_expansion`

$$\mathrm{e}^{\mathrm{i}u\sin\theta} = \sum_{n=-\infty}^{\infty} J_n(u)\mathrm{e}^{\mathrm{i}n\theta}$$

We proove for

$$\mathrm{e}^{-\mathfrak{B}+\mathfrak{B}^*} = \mathrm{e}^{-\mathrm{i}2|\mathfrak{B}|\sin\arg(-\mathfrak{B})},$$

which satisfies Jacobi-Anger expansion (3.15) since for us the sum is symmetrical around 0. Arguments of the exponential function above are equal for a complex number z and its complex conjugate z^*:

$$-z + z^* = |z|\mathrm{e}^{\mathrm{i}\varphi} - |z|\mathrm{e}^{-\mathrm{i}\varphi} = |z|(-\cos\varphi - \mathrm{i}\sin\varphi + \cos\varphi - \mathrm{i}\sin\varphi) = -\mathrm{i}2|z|\sin\varphi$$

$$-z = |z|\mathrm{e}^{\mathrm{i}\arg(-z)} \Rightarrow \varphi = \arg(-z)$$

List of Abbreviations

EM	Electromagnetic
TM	Transversal Magnetic
TE	Transversal Electric
SP	Surface Plasmon
SPs	Surface Plasmons
SPP	Surface Plasmon Polariton
SPPs	Surface Plasmon Polaritons
SPID	Surface Plasmon Interference Device
SEB	Shaped Electron Beam
SEBs	Shaped Electron Beams
PINEM	Photon-Induced Near-Field Electron Microscopy

BIBLIOGRAPHY

[1] AJIB, Rabih. Propagation of light in Plasmonic multilayers (2017). Available from INIS: http://inis.iaea.org/search/search.aspx?orig_q=RN:53042130.

[2] BERINI, Pierre. Long-range surface plasmon polaritons. *Advances in Optics and Photonics* [online]. 2009, 1(3) [cit. 2023-05-17]. ISSN 1943-8206. doi: 10.1364/AOP.1.000484

[3] DI GIULIO, Valerio and F. Javier GARCÍA DE ABAJO. Free-electron shaping using quantum light. *Optica*. 2020, 7(12). ISSN 2334-2536. doi: 10.1364/OPTICA.404598

[4] DVOŘÁK, Petr, Pavel KLOK, Michal KVAPIL, Martin HRTOŇ, Petr BOUCHAL, Jan KRPENSKÝ, Vlastimil KŘÁPEK and Tomá ŠIKOLA. Two-dimensional quantitative near-field phase imaging using square and hexagonal interference devices. *Nanophotonics*. 2022, 11(19), 4375-4386. ISSN 2192-8614. doi: 10.1515/nanoph-2022-0215

[5] DVOŘÁK, Petr, Tomáš NEUMAN, Lukáš BŘÍNEK, Tomáš ŠAMOŘIL, Radek KALOUSEK, Petr DUB, Peter VARGA and Tomá ŠIKOLA. Control and Near-Field Detection of Surface Plasmon Interference Patterns. *Nano Letters*. 2013, 13(6), 2558-2563. ISSN 1530-6984. doi: 10.1021/nl400644r

[6] DVOŘÁK, Petr, Zoltán ÉDES, Michal KVAPIL, et al. Imaging of near-field interference patterns by aperture-type SNOM influence of illumination wavelength and polarization state. *Optics Express*. 2017, 25(14). ISSN 1094-4087. doi: 10.1364/OE.25.016560

[7] FEYNMAN, Richard P. *QED: The Strange Theory of Light and Matter*. REV-Revised. Princeton University Press, 1985. ISBN 978-0691024172.

[8] GARCÍA DE ABAJO, F. Javier, Ana ASENJO-GARCIA and Mathieu KOCIAK. Multiphoton Absorption and Emission by Interaction of Swift Electrons with Evanescent Light Fields. *Nano Letters*. 2010, 10(5), 1859-1863. ISSN 1530-6984. doi: 10.1021/nl100613s

[9] GARCÍA DE ABAJO, F. Javier and Andrea KONEČNÁ. Optical Modulation of Electron Beams in Free Space. *Physical Review Letters*. 2021, 126(12). ISSN 0031-9007. doi: 10.1103/PhysRevLett.126.123901

[10] GARCÍA DE ABAJO, F. Javier and Valerio DI GIULIO. Optical Excitations with Electron Beams: Challenges and Opportunities. *ACS Photonics*. 2021, 8(4), 945-974. ISSN 2330-4022. doi: 10.1021/acsphotonics.0c01950

[11] GARCÍA DE ABAJO, F. Javier, Brett BARWICK and Fabrizio CARBONE. Electron diffraction by plasmon waves. *Physical Review B* [online]. 2016, 94(4) [cit. 2023-05-19]. ISSN 2469-9950. doi: 10.1103/PhysRevB.94.041404

[12] GRIFFITHS, David J. *Introduction to electrodynamics*. Fourth edition. Boston: Pearson, [2013]. ISBN 978-0-321-85656-2.

[13] HOHENESTER, Ulrich. *Nano and Quantum Optics: an Introduction to Basic Principles and Theory*. Cham: Springer, [2020]. Graduate texts in physics (Springer). ISBN 978-3-030-30503-1.

[14] KONEČNÁ, Andrea. *Theoretical description of low-energy excitations in nanostructures as probed by fast electrons*. Doctoral thesis. University of the Basque Country, (2019).

[15] KIRKLAND, Earl J. *Advanced computing in electron microscopy*. Second Edition. New York: Springer, [2010]. ISBN 978-1-4419-6532-5.

[16] KITTEL, Charles. *Introduction to solid state physics*. 8th ed. Hoboken: John Wiley, c2005. ISBN 978-0471415268.

[17] LIEBTRAU, Matthias, Murat SIVIS, Armin FEIST, et al. *Spontaneous and stimulated electronphoton interactions in nanoscale plasmonic near fields*. 2021, 10(1). ISSN 2047-7538. doi: 10.1038/s41377-021-00511-y

[18] LIU, Zhao-Wei, Qi-Huo WEI and Xiang ZHANG. Surface Plasmon Interference Nanolithography. *Nano Letters*. 2005, 5(5), 957-961. ISSN 1530-6984. doi: 10.1021/nl0506094

[19] MADAN, Ivan, Veronica LECCESE, Adam MAZUR, et al. Ultrafast Transverse Modulation of Free Electrons by Interaction with Shaped Optical Fields. *ACS Photonics*. 2022, 9(10), 3215-3224. ISSN 2330-4022. doi: 10.1021/acsphotonics.2c00850

[20] MAIER, Stefan A. *Plasmonics: fundamentals and applications*. New York: Springer, 2007. ISBN 0-387-33150-6.

[21] PARK, Sang Tae, Milo LIN and Ahmed H ZEWAIL. Photon-induced near-field electron microscopy (PINEM): theoretical and experimental. *New Journal of Physics*. 2010, 12(12). ISSN 1367-2630. doi: 10.1088/1367-2630/12/12/123028

[22] PIAZZA, Luca, Tom T.A. LUMMEN, et al. Simultaneous observation of the quantization and the interference pattern of a plasmonic near-field. *Nature Communications*. 2015, 6(1). ISSN 2041-1723. doi: 10.1038/ncomms7407

[23] RENGER, Jan, Stefan GRAFSTRÖM and Lukas M. ENG. Direct excitation of surface plasmon polaritons in nanopatterned metal surfaces and thin films. *Physical Review B*. 2007, 76(4). ISSN 1098-0121. doi: 10.1103/PhysRevB.76.045431

[24] TSESSES, Shai, et al. Optical skyrmion lattice in evanescent electromagnetic fields. *Science*. 2018, 361(6406), 993-996. ISSN 0036-8075. doi: 10.1126/science.aau0227

[25] TSESSES, Shai, Raphael DAHAN, Kangpeng WANG, Tomer BUCHER, Kobi COHEN, Ori REINHARDT, Guy BARTAL and Ido KAMINER. Tunable photon-induced spatial modulation of free electrons. *Nature Materials*. 2023, 22(3), 345-352. ISSN 1476-1122. doi: 10.1038/s41563-022-01449-1

[26] VANACORE, Giovanni Maria, Ivan MADAN, Gabriele BERRUTO, et al. Attosecond coherent control of free-electron wave functions using semi-infinite light fields. *Nature Communications*. 2018, 9(1). ISSN 2041-1723. doi: 10.1038/s41467-018-05021-x

[27] ZHANG, Junxi, Lide ZHANG and Wei XU. Surface plasmon polaritons: physics and applications. *Journal of Physics D: Applied Physics*. 2012, 45(11). ISSN 0022-3727. doi: 10.1088/0022-3727/45/11/113001